

Constraint Learning in Multi-Agent Dynamic Games from Demonstrations of Local Nash Interactions

Zhouyu Zhang^{1*} and Chih-Yuan Chiu^{1*} and Glen Chou¹

Abstract—We present an inverse dynamic game-based algorithm to learn parametric constraints from a given dataset of local Nash equilibrium interactions between multiple agents. Specifically, we introduce mixed-integer linear programs (MILP) encoding the Karush-Kuhn-Tucker (KKT) conditions of the interacting agents, which recover constraints consistent with the local Nash stationarity of the interaction demonstrations. We establish theoretical guarantees that our method learns inner approximations of the true safe and unsafe sets. We also use the interaction constraints recovered by our method to design motion plans that robustly satisfy the underlying constraints. Across simulations and hardware experiments, our methods accurately inferred constraints and designed safe interactive motion plans for various classes of constraints, both convex and non-convex, from interaction demonstrations of agents with nonlinear dynamics.

1. INTRODUCTION

Learning from demonstrations (LfD) is a powerful paradigm for enabling robots to learn constraints in their workspace [1]–[3]. In particular, [1], [2] formulate constraint inference as identifying the parameters that best explain a set of approximately optimal demonstration trajectories. However, existing methods assume robots operate in isolation, and thus cannot infer coupled constraints that depend on the states or controls of multiple agents, e.g., collision avoidance, which cannot be easily encoded using cost function penalties.

To address this gap, we use tools from dynamic game theory and inverse optimal control (IOC) to learn constraints from the demonstrations of *interactions* between multiple strategic agents. We recover unknown constraint parameters by posing an inverse optimization problem that uses Nash equilibrium constraints to encode steady-state agent interactions and show that the inferred constraints can be used for robust motion planning. Although IOC and dynamic games have been applied for *cost* inference in multi-agent settings [4]–[7], to our knowledge, our work designs the first game-theoretic algorithm for multi-agent *constraint* inference that is *guaranteed* to either recover or conservatively estimate the true constraint set. Our main contributions are:

- 1) We formulate a feasibility problem to learn parameterized constraints from multi-agent interaction demonstrations, generalizing the method in [1] to the multi-agent setting. Under mild conditions, we prove that our method learns conservative estimates of the true safe and unsafe sets.
- 2) We use our framework to extract volumes of provably safe or unsafe trajectories, or reject volumes of the constraint parameter space incompatible with the demonstrations.

*Equal contribution.

¹Schools of ECE, AE, and CSP, Georgia Institute of Technology.

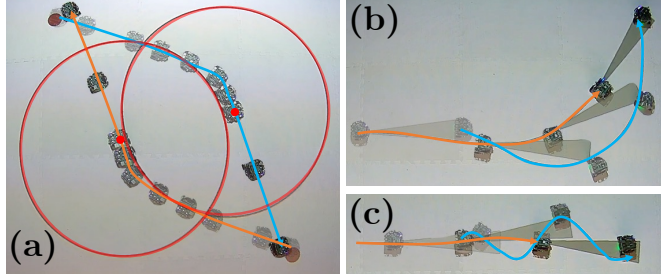


Fig. 1: Time-lapse of safe plans computed for ground robots (Sec. V-C) using (a) spherical collision-avoidance constraints (red circles) learned via our method; opacity increases over time; (b-c) learned line-of-sight constraints: the leading agent (blue) follows a (b) half-circle or (c) sinusoid; the pursuer (orange) maintains line-of-sight (shaded area).

This volume extraction approach enables safe motion planning that is robust to constraint ambiguity. We also establish fundamental limitations of the learnability of interaction constraints from demonstrations.

- 3) We evaluate our method in simulation and hardware experiments where agents with nonlinear dynamics interact under collision avoidance, line-of-sight, and proximity constraints. Our inverse learning and planning algorithms recovered unknown constraint parameters and generated safe motion plans robust to constraint uncertainty. In contrast, naive applications of the baseline single-agent constraint inference method in [1] failed to accurately recover unknown constraints with zero stationarity error (Sec. V-D). Moreover, cost-inference based methods which encode constraints as log barrier costs were unable to recover constraint information that could be used to generate safe motion plans downstream (Sec. V-H).

Due to space, the appendix (with proofs, discussion, further experiments) is in an extended version of this paper [8].

II. RELATED WORK

A. Constraint Learning via Inverse Optimal Control (IOC)

LfD via IOC has been applied to enable robots to learn new tasks [9], [10], infer the intent of other strategic agents [4]–[6], and recover static environment constraints [1], [11]. In particular, [10] leverages IOC to infer convex constraints from a finite set of possible costs and constraints, while [12]–[14] use a single demonstration to infer local trajectory-level constraints. Our method is closest to [1], which recovers unknown constraint parameters by enforcing the KKT conditions of a set of locally optimal demonstrations. However, these methods focus on single-agent scenarios. In contrast,

we use demonstrations of strategic multi-agent interactions to infer constraints coupled across agent states and controls.

B. Forward and Inverse Dynamic Games

Motion planning and intent inference in multi-agent scenarios are naturally posed as dynamic games [15], which provide a powerful theoretical framework for reasoning about strategic multi-robot interactions. Computationally tractable algorithms for approximating general-sum *forward dynamic games* have been developed [6], [16]–[19], enabling efficient motion planning in interactive scenarios. Meanwhile, [4]–[7], [20] developed *inverse dynamic game* algorithms that infer unknown agent costs from interaction demonstrations via KKT conditions encoding local Nash stationarity. Other works focus on inferring information structure [21] or foresightedness [22] from interactions at or near local Nash stationarity. However, most existing inverse game-theoretic methods are not directly applicable to *constraint* inference. Exceptions include [23], which infers *a priori* unknown parameters for agent costs and constraints from a finite set of hypotheses, and [24], which produces posterior distributions over such parameters. Unlike [23], [24], our method explicitly searches over a continuous parameter space, and is guaranteed to learn an inner approximation of the true constraint set.

III. DYNAMIC GAMES AND PROBLEM STATEMENT

Consider an N -agent, T -stage discrete-time *forward dynamic game* \mathcal{G} , in which $x_t^i \in \mathbb{R}^{n_i}$ is the state vector of each agent $i \in [N] := \{1, \dots, N\}$ at each time $t \in [T] := \{1, \dots, T\}$. We define $x_t := (x_t^1, \dots, x_t^N) \in \mathbb{R}^n$ and $u_t := (u_t^1, \dots, u_t^N) \in \mathbb{R}^m$ for each $t \in [T]$, where $n := \sum_{i \in [N]} n_i$ and $m := \sum_{i \in [N]} m_i$, and $x := (x_1, \dots, x_T) \in \mathbb{R}^{nT}$ and $u := (u_1, \dots, u_T) \in \mathbb{R}^{mT}$. Finally, we define $\xi := (x, u) \in \mathbb{R}^{(n+m)T}$ to be the system's state-control trajectory.

Each agent $i \in [N]$ aims to minimize its cost $J^i(\xi)$, whose value depends on the system trajectory ξ . Moreover, the trajectory of each agent $i \in [N]$ must ensure that the scalar equality constraints $C^{\text{eq},i} := \{h_\beta^i(\xi) = 0 : \beta \in [N^{\text{eq},i}]\}$, and scalar inequality constraints $C_k^{\text{ineq},i} := \{g_{\beta,k}^i(\xi) \leq 0 : \beta \in [N_k^{\text{ineq},i}]\}$ and $C_{\gamma_k}^{\text{ineq},i} := \{g_{\beta,\gamma_k}^i(\xi, \theta^*) \leq 0 : \beta \in [N_{\gamma_k}^{\text{ineq},i}]\}$ are satisfied,¹ where $N^{\text{eq},i}$, $N_k^{\text{ineq},i}$, and $N_{\gamma_k}^{\text{ineq},i}$ are the number of scalar constraints in $C^{\text{eq},i}$, $C_k^{\text{ineq},i}$, and $C_{\gamma_k}^{\text{ineq},i}$, respectively. Above, the constraint $g_{\beta,\gamma_k}^i(\cdot, \theta^*)$ is parameterized by the parameter $\theta^* \in \Theta$, while Θ is a compact set of all possible parameter values². We stack constraint functions $g_{\beta,k}^i$, g_{β,γ_k}^i , and h_β^i across all $\beta \in [N]$ to form \mathbf{g}_k^i , $\mathbf{g}_{\gamma_k}^i$, and \mathbf{h}^i , respectively, for each agent $i \in [N]$. We further stack across all $i \in [N]$ to form \mathbf{g}_k , \mathbf{g}_{γ_k} , and \mathbf{h} , respectively. Moreover, we write $\mathbf{g}(\theta, \xi) = (\mathbf{g}_k(\xi), \mathbf{g}_{\gamma_k}(\xi, \theta))$.

¹We assume all unknown constraints are *inequality* constraints. An unknown equality constraint $h_\beta^i(\xi, \theta) = 0$ can be inferred using \mathcal{D} via regression analysis and root-finding methods, or expressed as two inequality constraints ($h_\beta^i(\xi, \theta) \leq 0$ and $-h_\beta^i(\xi, \theta) \leq 0$) and learned via our method.

²Our methods readily extend to the case where each agent's constraint set is the *union of intersections* of equality and inequality constraints. For simplicity, our formulation here considers only *intersections*.

The constraints $\mathbf{h}^i(\cdot)$ and $\mathbf{g}^i(\cdot)$ for each agent $i \in [N]$ encode the system dynamics $x_{t+1}^i = f_t(x_t^i, u_t^i)$ constraining the motion of each agent, as well as obstacle avoidance, inter-agent collision avoidance, and other constraints. Finally, for any parameter value $\theta \in \Theta$, we denote by $\mathcal{S}(\theta)$ (resp., $\mathcal{A}(\theta)$) the set of all trajectories satisfying (resp., violating) the inequality constraints $\mathbf{g}_{\gamma_k}(\xi, \theta) \leq 0$, i.e.,

$$\mathcal{S}(\theta) := \bigcap_{i \in [N]} \{\xi \in \mathbb{R}^{(n+m)T} : \mathbf{g}_{\gamma_k}(\xi, \theta) \leq 0\}, \quad (1)$$

$$\mathcal{A}(\theta) := \mathcal{S}(\theta)^c. \quad (2)$$

The objective of the *forward dynamic game* is to compute the interactive system trajectory by solving the following coupled optimization problems for each agent $i \in [N]$:

$$\min_{x^i, u^i} \quad J^i(\xi) \quad (3a)$$

$$\text{s.t.} \quad h_\beta^i(\xi) = 0, \quad \forall \beta \in [N^{\text{eq},i}], \quad (3b)$$

$$g_{\beta,k}^i(\xi) \leq 0, \quad \forall \beta \in [N_k^{\text{ineq},i}], \quad (3c)$$

$$g_{\beta,\gamma_k}^i(\xi, \theta^*) \leq 0, \quad \forall \beta \in [N_{\gamma_k}^{\text{ineq},i}]. \quad (3d)$$

We call u^* a *Nash equilibrium solution* to (3) with state trajectory x^* if the state-control trajectory $\xi^* := (x^*, u^*)$ satisfies (3). We call u^* a *local Nash equilibrium solution* to (3) with trajectory x^* if $\xi^* := (x^*, u^*) \in \mathbb{R}^{(n+m)T}$ satisfies the following: There exists a neighborhood $\mathcal{N}(\xi^*)$ of ξ^* such that for any agent $i \in [N]$ and any feasible state-control trajectory $\{(x_t^i, u_t^i) : t \in [T]\}$ of agent i in $\mathcal{N}(\xi^*)$, we have $J^i(\xi^*) = J^i(x^*, u^*) \leq J^i(x^{i*}, u^{i*}, x^{-i*}, u^{-i*}) := J^i(\xi^i, \xi^{-i*})$, where $-i$ refers to all indices in $[N]$ apart from i .

Problem Statement: Assuming $\{J^i(\cdot) : i \in [N]\}$, $\mathbf{g}_k(\cdot)$, $\mathbf{g}_{\gamma_k}(\cdot, \cdot)$, $\mathbf{h}_k(\cdot)$, and Θ are known, we aim to infer θ^* from a set of D local Nash equilibrium demonstrations $\mathcal{D} := \{\xi_d^{\text{loc}} : d \in [D]\}$, and leverage the learned constraint information to design safe interactive motion plans.

IV. MULTI-AGENT CONSTRAINT INFERENCE AND ROBUST MOTION PLANNING

Below, we formulate our constraint inference problem using KKT conditions derived from the forward dynamic game (4) (Sec. IV-A). We illustrate that the problem of learning *offset-parameterized interaction constraints* in dynamic games, e.g., various collision-avoidance constraints, can be reformulated as MILPs (Sec. IV-B). Then, we present methods for extracting guaranteed safe and unsafe trajectories, rejecting parameter values inconsistent with the demonstrated interactions, and using the extracted knowledge to design safe plans under constraint uncertainty (Sec. IV-C). Finally, we present fundamental limitations of learning interaction constraints from demonstrations (Sec. IV-D).

A. KKT Conditions for Multi-Agent Constraint Inference

Since each interaction demonstration ξ_d^{loc} in \mathcal{D} is at local Nash equilibrium, it must satisfy the KKT conditions associated with (3). Thus, for each $\xi_d^{\text{loc}} \in \mathcal{D}$, there exist Lagrange multipliers $\boldsymbol{\lambda}_{d,k}^i := \{\lambda_{d,\beta,k}^i, \forall \beta \in [N_k^{\text{ineq},i}]\}$, $\boldsymbol{\lambda}_{d,\gamma_k}^i := \{\lambda_{d,\beta,\gamma_k}^i, \forall \beta \in [N_{\gamma_k}^{\text{ineq},i}]\}$, and $\boldsymbol{\nu}_d^i := \{\nu_{d,\beta}^i, \forall \beta \in [N^{\text{eq},i}]\}$

satisfying the following equations with $\theta = \theta^*$, $\xi = \xi_d^{\text{loc}}$:

$$\mathbf{h}^i(\xi) = 0, \quad \mathbf{g}_k^i(\xi) \leq 0, \quad \mathbf{g}_{\gamma_k}^i(\xi, \theta) \leq 0, \quad (4a)$$

$$\boldsymbol{\lambda}_{d,k}^i, \boldsymbol{\lambda}_{d,\gamma_k}^i \geq 0, \quad (4b)$$

$$\boldsymbol{\lambda}_{d,k}^i \odot \mathbf{g}_k^i(\xi) = 0, \quad \boldsymbol{\lambda}_{d,\gamma_k}^i \odot \mathbf{g}_{\gamma_k}^i(\xi, \theta) = 0, \quad (4c)$$

$$\nabla_{\xi^i} J^i(\xi) + (\boldsymbol{\lambda}_{d,k}^i)^\top \nabla_{\xi^i} \mathbf{g}_k^i(\xi) \quad (4d)$$

$$+ (\boldsymbol{\lambda}_{d,\gamma_k}^i)^\top \nabla_{\xi^i} \mathbf{g}_{\gamma_k}^i(\xi, \theta) + (\boldsymbol{\nu}_d^i)^\top \nabla_{\xi^i} \mathbf{h}^i(\xi) = 0.$$

Here, \odot denotes element-wise multiplication, and ∇ defines the gradient of any differentiable function $\mathbf{f} : \mathbb{R}^n \rightarrow \mathbb{R}^m$, i.e., $[\nabla_x \mathbf{f}]_{i'j'} := \frac{\partial f_{i'}}{\partial x_{j'}}$ for each $i' \in [m]$ and $j' \in [n]$. Above, (4a) encodes primal feasibility, (4b) encodes dual feasibility, (4c) encodes complementary slackness, while (4d) encodes first-order KKT stationarity. We concatenate the dual variables $\boldsymbol{\lambda}_{d,k}^i$, $\boldsymbol{\lambda}_{d,\gamma_k}^i$, and $\boldsymbol{\nu}_d^i$ across $d \in [D]$ to form $\boldsymbol{\lambda}_k^i$, $\boldsymbol{\lambda}_{\gamma_k}^i$, and $\boldsymbol{\nu}^i$, respectively, and we further concatenate across $i \in [N]$ to form $\boldsymbol{\lambda}_k$, $\boldsymbol{\lambda}_{\gamma_k}$, and $\boldsymbol{\nu}$, respectively. We also define:

$$\begin{aligned} \text{KKT}^i(\xi_d^{\text{loc}}) &:= \{(\theta, \boldsymbol{\lambda}_k, \boldsymbol{\lambda}_{\gamma_k}, \boldsymbol{\nu}) : (\theta, \boldsymbol{\lambda}_{d,k}^i, \boldsymbol{\lambda}_{d,\gamma_k}^i, \boldsymbol{\nu}_d^i) \\ &\quad \text{satisfies (4) with } \xi = \xi_d^{\text{loc}}\}, \end{aligned} \quad (5)$$

$$\text{KKT}(\mathcal{D}) := \bigcap_{i \in [N]} \bigcap_{d \in [D]} \text{KKT}^i(\xi_d^{\text{loc}}). \quad (6)$$

Conversely, we say that $\xi \in \mathbb{R}^{(n+m)T}$ is at *local Nash stationarity* with respect to the underlying constraints $\mathbf{h}(\cdot)$, $\mathbf{g}_k(\cdot)$, and $\mathbf{g}_{\gamma_k}(\cdot, \theta)$ if there exist $\boldsymbol{\nu}$, $\boldsymbol{\lambda}_k$, and $\boldsymbol{\lambda}_{\gamma_k}$ such that $(\theta, \boldsymbol{\lambda}_k, \boldsymbol{\lambda}_{\gamma_k}, \boldsymbol{\nu}) \in \text{KKT}(\{\xi\})$.

Given the set \mathcal{D} of local Nash equilibrium demonstrations, there must exist Lagrange multipliers $\{\boldsymbol{\lambda}_{d,k}^{i^*}, \boldsymbol{\lambda}_{d,\gamma_k}^{i^*}, \boldsymbol{\nu}_d^{i^*} : i \in [N], d \in [D]\}$ such that $(\theta^*, \boldsymbol{\lambda}_k^{i^*}, \boldsymbol{\lambda}_{\gamma_k}^{i^*}, \boldsymbol{\nu}^{i^*})$ solves:

$$\text{find } \theta, \boldsymbol{\lambda}_k, \boldsymbol{\lambda}_{\gamma_k}, \boldsymbol{\nu}, \quad (7a)$$

$$\text{s.t. } (\theta, \boldsymbol{\lambda}_k, \boldsymbol{\lambda}_{\gamma_k}, \boldsymbol{\nu}) \in \text{KKT}(\mathcal{D}). \quad (7b)$$

Conversely, the solution set of (7) encodes parameter values θ consistent with the local Nash stationarity of \mathcal{D} , and contains the true parameter value θ^* . We denote by $\mathcal{F}(\mathcal{D})$ the set of parameter values compatible with $\text{KKT}(\mathcal{D})$, i.e.,

$$\begin{aligned} \mathcal{F}(\mathcal{D}) &:= \{\theta \in \Theta : \exists \boldsymbol{\lambda}_k, \boldsymbol{\lambda}_{\gamma_k}, \boldsymbol{\nu} \text{ s.t.} \\ &\quad (\theta, \boldsymbol{\lambda}_k, \boldsymbol{\lambda}_{\gamma_k}, \boldsymbol{\nu}) \in \text{KKT}(\mathcal{D})\}. \end{aligned} \quad (8)$$

Thm. 1 below establishes that the ground truth safe set $\mathcal{S}(\theta^*)$ is guaranteed to be inner (i.e., conservatively) approximated by the set of all trajectories satisfying $\mathbf{g}(\xi, \theta) \leq 0$ for all $\theta \in \mathcal{F}(\mathcal{D})$. Similarly, the ground truth avoid set $\mathcal{A}(\theta^*)$ is guaranteed to be inner approximated by the set of all trajectories violating $\mathbf{g}(\xi, \theta) \leq 0$ for all $\theta \in \mathcal{F}(\mathcal{D})$.

Theorem 1: (Conservativeness of Safe and Unsafe Set Recovery from (7)) Define the learned set of *guaranteed safe* (resp., *unsafe*) trajectories, denoted by $\mathcal{G}_s(\mathcal{D})$ (resp., $\mathcal{G}_{\gamma_s}(\mathcal{D})$), to be the set of trajectories that are safe (resp., unsafe) with respect to all parameters $\theta \in \mathcal{F}(\mathcal{D})$, i.e.,³

$$\mathcal{G}_s(\mathcal{D}) := \bigcap_{\theta \in \mathcal{F}(\mathcal{D})} \{\xi \in \mathbb{R}^{(n+m)T} : \mathbf{g}(\xi, \theta) \leq 0\}, \quad (9)$$

$$\mathcal{G}_{\gamma_s}(\mathcal{D}) := \bigcap_{\theta \in \mathcal{F}(\mathcal{D})} \{\xi \in \mathbb{R}^{(n+m)T} : \mathbf{g}(\xi, \theta) > 0\}. \quad (10)$$

³Note that $\mathcal{G}_{\gamma_s}(\mathcal{D}) \neq \mathcal{G}_s(\mathcal{D})^c$, i.e., it is possible for a given trajectory to be neither guaranteed safe nor guaranteed unsafe.

Then $\mathcal{G}_s(\mathcal{D}) \subseteq \mathcal{S}(\theta^*)$ and $\mathcal{G}_{\gamma_s}(\mathcal{D}) \subseteq \mathcal{A}(\theta^*)$.

Proof: By definition of $\mathcal{G}_s(\mathcal{D})$ in (9) and $\mathcal{S}(\theta)$ in (1), $\mathcal{G}_s(\mathcal{D}) = \bigcap_{\theta \in \mathcal{F}(\mathcal{D})} \mathcal{S}(\theta)$. Thus, to prove $\mathcal{G}_s(\mathcal{D}) \subseteq \mathcal{S}(\theta^*)$, it suffices to verify that $\theta^* \in \mathcal{F}(\mathcal{D})$. Since \mathcal{D} contains local Nash equilibrium trajectories of the dynamic game with constraints parameterized by θ^* , for any $\xi_d \in \mathcal{D}$, there exist $\boldsymbol{\lambda}_{d,k}, \boldsymbol{\lambda}_{d,\gamma_k}, \boldsymbol{\nu}_d$ such that $(\theta^*, \boldsymbol{\lambda}_{d,k}, \boldsymbol{\lambda}_{d,\gamma_k}, \boldsymbol{\nu}_d) \in \text{KKT}(\{\xi_d\})$. Thus, $\theta^* \in \mathcal{F}(\mathcal{D})$, so $\mathcal{G}_s(\mathcal{D}) \subseteq \mathcal{S}(\theta^*)$. Similarly, by definition of $\mathcal{G}_{\gamma_s}(\mathcal{D})$ in (10) and $\mathcal{A}(\theta)$ in (2), $\mathcal{G}_{\gamma_s}(\mathcal{D}) = \bigcap_{\theta \in \mathcal{F}(\mathcal{D})} \mathcal{A}(\theta)$. Thus, to prove $\mathcal{G}_{\gamma_s}(\mathcal{D}) \subseteq \mathcal{A}(\theta^*)$, it suffices to verify $\theta^* \in \mathcal{F}(\mathcal{D})$, which we have done above. ■

For many constraints (e.g., collision-avoidance), the primal feasibility conditions (4a) restrict the relative agent positions $\{x_t^j - x_t^i : \forall i, j \in [N], j \neq i, \forall t \in [T]\}$ to lie inside a constraint set characterized by a union of polytopes. In this case, (7) can be reformulated as a mixed-integer linear program (MILP) or a mixed-integer bilinear program (MIBLP), and solved via off-the-shelf solvers [25] (see Sec. IV-B and App. B). The difference in the optimization problem class depends on the parameterization of the unknown constraint.

Remark 1: If the given demonstrations are not at local Nash stationarity, we relax the stationarity condition (4d) in (7b) into a cost defined using the following stationarity terms:

$$\begin{aligned} \text{stat}^i(\xi_d^{\text{loc}}, \theta) &:= \nabla_{\xi^i} J^i(\xi) + (\boldsymbol{\lambda}_{d,k}^i)^\top \nabla_{\xi^i} \mathbf{g}_k^i(\xi) \\ &\quad + (\boldsymbol{\lambda}_{d,\gamma_k}^i)^\top \nabla_{\xi^i} \mathbf{g}_{\gamma_k}^i(\xi, \theta) + (\boldsymbol{\nu}_d^i)^\top \nabla_{\xi^i} \mathbf{h}^i(\xi) \end{aligned} \quad (11)$$

across all $d \in [D]$ and $i \in [N]$. Concretely, we relax (7) into the following optimization program:

$$\min_{\theta, \boldsymbol{\lambda}_k, \boldsymbol{\lambda}_{\gamma_k}, \boldsymbol{\nu}} \sum_{d \in [D]} \sum_{i \in [N]} \|\text{stat}^i(\xi_d^{\text{loc}}, \theta)\|_1, \quad (12a)$$

$$\text{s.t. } (4a) - (4c), \quad i \in [N], d \in [D]. \quad (12b)$$

Remark 2: Even with *inaccurate* knowledge of the constraint parameterization, the constraint learner may still approximate constraints effectively by selecting a base constraint shape (e.g., polytope) as a building block, and incrementally introducing more base shapes until the stationarity error (12a) is sufficiently small. (see Sec. V-F and Fig. 6).

B. MILP Reformulation for Unions of Offset-Parameterized Constraints

Suppose all agents have equal state dimension (i.e., $n_i = n_j \forall i, j \in [N]$), and the unknown constraints $\mathbf{g}_{\gamma_k}^i(\xi, \theta) \leq 0$ encode that $\forall t \in [T]$, the state of each other agent $j \in [N] \setminus \{i\}$ relative to agent i lies outside a polytopic collision avoidance set with N_c sides, each of which is represented as a scalar constraint. Concretely, feasible system-level trajectories must lie outside avoid sets:

$$\mathcal{A}^{i,j,t}(\theta^*) := \bigcap_{\beta=1}^{N_c} \{\xi \in \mathbb{R}^{(n+m)T} : \mathbf{a}_\beta^{i,j,t\top} \xi < b_\beta^i(\theta^*)\} \quad (13)$$

for all $i, j \in [N]$, $j \neq i$, $t \in [T]$, where $\mathbf{a}_\beta^{i,j,t} \in \mathbb{R}^{(n+m)T}$, $b_\beta^i(\theta^*) \in \mathbb{R}$, $\forall i, j \in [N]$, $j \neq i$, $t \in [T]$, and each $b_\beta^i(\theta^*)$ is specified by an unknown parameter θ^* . Thus, trajectories ξ must evade the avoid set:

$$\mathcal{A}(\theta^*) := \bigcup_{i,j \in [N], j \neq i, t \in [T]} \mathcal{A}^{i,j,t}(\theta^*), \quad (14)$$

or equivalently, stay within the safe set $\mathcal{S}(\theta^*) := (\mathcal{A}(\theta^*))^c$:

$$\mathcal{S}(\theta^*) := \bigcap_{i,j \in [N], j \neq i, t \in [T]} \bigcup_{\beta \in [N_c]} \{\xi : \mathbf{a}_\beta^{i,j,t\top} \xi \geq b_\beta^i(\theta^*)\} \quad (15)$$

To recover θ^* , we now reformulate the KKT conditions (4) as an MILP by extending the approach of [1, Sec. IV-B] to accommodate our multi-agent constraint learning problem. For notational ease, in the rest of Sec. IV-B, we focus on learning interaction constraints between $N = 2$ agents from a single demonstration ξ^{loc} (i.e., $D = 1$). We set $\mathbf{a}_\beta^{i,t} := \mathbf{a}_\beta^{i,3-i,t}$ and $\mathcal{A}^{i,t}(\theta^*) := \mathcal{A}^{i,3-i,t}(\theta^*) \forall i \in [2], t \in [T]$. For a treatment without the above restrictions, see App. B.

1) Reformulating primal feasibility (4a):

First, we rewrite (4a) via the big-M formulation [1], [26], by introducing binary vectors $\mathbf{z}^{i,t} = (z_\beta^{i,t} \in \{0, 1\} : \beta \in [N_c]) \in \{0, 1\}^{N_c}$, for each $i \in [2], t \in [T]$, as follows — $\forall i \in [2], t \in [T]$:

$$(\mathbf{A}^{i,t})^\top \xi^{\text{loc}} \geq \mathbf{b}^{i,t}(\theta) - M(\mathbf{1}_{N_c} - \mathbf{z}^{i,t}), \quad (16a)$$

$$\sum_{\beta=1}^{N_c} z_\beta^{i,t} \geq 1, \quad (16b)$$

Above, $M \gg 0$, $\mathbf{1}_{N_c} := (1, \dots, 1) \in \mathbb{R}^{N_c}$, while $\mathbf{A}^{i,t} \in \mathbb{R}^{(n+m)T \times N_c}$ and $\mathbf{b}^{i,t}(\theta) \in \mathbb{R}^{N_c}$ are the concatenations of $\mathbf{a}_\beta^{i,t}$ and $b_\beta^{i,t}(\theta)$, respectively, across all $\beta \in [N_c]$.

2) Reformulating complementary slackness (4c):

Let $\boldsymbol{\lambda}_{\gamma_k}^{i,t} = (\lambda_{\beta, \gamma_k}^{i,t} \geq 0 : \beta \in [N_c]) \in \mathbb{R}^{N_c}$ denote the dual variables associated with the inequalities $(\mathbf{a}_\beta^{i,t})^\top \xi \geq b_\beta^{i,t}(\theta)$, across $\beta \in [N_c]$. Since the safe set definition (15) involves a union over $\beta \in [N_c] \forall i \in [2], t \in [T]$, the constraint $\{\xi \in \mathbb{R}^{(n+m)T} : (\mathbf{a}_\beta^{i,t})^\top \xi^{\text{loc}} \geq b_\beta^{i,t}(\theta)\}$, for each $i \in [2], t \in [T]$, might only be enforced for a strict subset of the indices $\beta \in [N_c]$, which we denote by $\mathcal{B}^{i,t} \subseteq [N_c]$. Likewise, $\forall i \in [2], t \in [T]$, complementary slackness (4c) should only be enforced for indices in $\mathcal{B}^{i,t}$, and in turn, terms of the form $\lambda_{\beta, \gamma_k}^{i,t} \nabla_{\xi^{i,t}} g_{\beta, \gamma_k}(\xi, \theta)$ are only included in the stationarity condition (4d) if $\beta \in \mathcal{B}^{i,t}$. Thus, we use a big-M formulation, in which we introduce binary vectors $\hat{\mathbf{z}}_1^{i,t} = (\hat{z}_{1,\beta}^{i,t} : \beta \in [N_c]) \in \{0, 1\}^{N_c}$ and $\hat{\mathbf{z}}_2^{i,t} = (\hat{z}_{2,\beta}^{i,t} : \beta \in [N_c]) \in \{0, 1\}^{N_c}$ to encode (4c), and binary vectors $\mathbf{q}^{i,t} = (q_\beta^{i,t} : \beta \in [N_c]) \in \{0, 1\}^{N_c}$ to enforce (4c). Concretely, we rewrite the complementary slackness conditions (4c) as follows — $\forall i \in [2], t \in [T]$:

$$\left[\mathbf{A}^{i,t\top} \xi^{\text{loc}} - \mathbf{b}^{i,t}(\theta) \right] \leq M \begin{bmatrix} \hat{z}_1^{i,t} \\ \hat{z}_2^{i,t} \end{bmatrix}, \quad (17a)$$

$$\hat{z}_{1,\beta}^{i,t} + \hat{z}_{2,\beta}^{i,t} \leq 2 - q_\beta^{i,t}, \quad \forall \beta \in [N_c], \quad (17b)$$

$$\sum_{\beta'=1}^{N_c} q_{\beta'}^{i,t} \geq 1. \quad (17c)$$

3) Reformulating stationarity (4d):

As noted above, the stationarity condition (4d) includes the term $\lambda_{\beta, \gamma_k}^{i,t} \nabla_{\xi^{i,t}} g_{\beta, \gamma_k}(\xi, \theta)$ only if $\beta \in \mathcal{B}^{i,t}$. To enforce this condition, $\forall i \in [2], t \in [T]$, we define $L^{i,t} \in \mathbb{R}^{N_c \times (n_i+m_i)T}$ as the matrix whose β -th row equals $\lambda_{\beta, \gamma_k}^{i,t} \nabla_{\xi^{i,t}} (b_\beta^{i,t}(\theta) - \mathbf{a}_\beta^{i,t\top} \xi)|_{\xi=\xi^{\text{loc}}}$. We

then rewrite the term $\boldsymbol{\lambda}_{\gamma_k}^{i,t\top} \nabla_{\xi^{i,t}} \mathbf{g}_{\gamma_k}^{i,t}(\xi, \theta)$ in (4d) as follows — $\forall i \in [2]$:

$$\begin{aligned} & \sum_{t \in [T]} \boldsymbol{\lambda}_{\gamma_k}^{i,t\top} \nabla_{\xi^{i,t}} (b^{i,t}(\theta) - \mathbf{A}^{i,t\top} \xi)^\top |_{\xi=\xi^{\text{loc}}} \quad (18) \\ &= \sum_{t \in [T]} \mathbf{q}^{i,t\top} L^{i,t}. \end{aligned}$$

By replacing the bilinear terms $\mathbf{q}^{i,t\top} L^{i,t}$ in (18) with slack variables and adding constraints, we can reformulate (18) in a linear manner. Concretely, $\forall i \in [2], t \in [T]$, we define $\tilde{q}^{i,t} := 1 - \mathbf{q}^{i,t}$ and introduce slack variables $R^{i,t} \in \mathbb{R}^{N_c \times (n_i+m_i)}$. Let $R_{\beta,\ell}^{i,t}$ and $L_{\beta,\ell}^{i,t}$ denote the $(\beta\text{-th row}, \ell\text{-th column})$ entry of $R^{i,t}$ and $L^{i,t}$, respectively, $\forall \beta \in [N_c], \ell \in [n]$. We assume each $L_{\beta,\ell}^{i,t}$ is component-wise bounded below and above by some \underline{M} and \overline{M} , respectively. We then introduce the constraints below, $\forall \beta \in [N_c], \ell \in [n]$, to linearize $\mathbf{q}^{i,t\top} L^{i,t}$:

$$\min\{0, \underline{M}\} \leq R_{\beta,\ell}^{i,t} \leq \overline{M}, \quad (19a)$$

$$M q_\beta^{i,t} \leq R_{\beta,\ell}^{i,t} \leq \overline{M} q_\beta^{i,t}, \quad (19b)$$

$$L_{\beta,\ell}^{i,t} - \tilde{q}_\beta^{i,t} \overline{M} \leq R_{\beta,\ell}^{i,t} \leq L_{\beta,\ell}^{i,t} - \tilde{q}_\beta^{i,t} \underline{M} \quad (19c)$$

$$R_{\beta,\ell}^{i,t} \leq L_{\beta,\ell}^{i,t} + \tilde{q}_\beta^{i,t} \overline{M} \quad (19d)$$

C. Volume Extraction Over Trajectories and Parameters for Motion Planning

When the given demonstrations are insufficiently informative to allow the unambiguous recovery of the true constraint parameter θ^* , an incorrect point estimate of θ^* may cause motion plans generated downstream to be unsafe (Sec. V, Fig. 10 in App. E.4 [8]). To address this issue, we describe methods to recover inner approximations of the guaranteed safe set $\mathcal{G}_s(\mathcal{D})$, by extracting *volumes* of guaranteed safe trajectories from a set of queried trajectories (Thm. 2) or parameter values (Thm. 3). Strategies for querying trajectories or constraint parameters are provided in Remark 3.

Theorem 2 (Volume Extraction Over Trajectories):

Given a set of queried trajectories $\mathcal{Q}_\xi := \{\xi_q \in \mathbb{R}^{(n+m)T} : q \in [Q_\xi]\}$, for each $\xi_q \in \mathcal{Q}_\xi$, define:

$$\epsilon_q := \min_{\theta \in \mathcal{F}(\mathcal{D}), \xi} \cdot \|\xi - \xi_q\|_\infty \quad (20a)$$

$$\text{s.t. } \mathbf{g}(\xi, \theta) > 0. \quad (20b)$$

For each $\xi_q \in \mathcal{Q}_\xi$, let $B_{\epsilon_q}^\infty(\xi_q)$ be the open ∞ -norm neighborhood of radius ϵ_q centered at ξ_q . Then:

$$\bigcup_{\xi_q \in \mathcal{Q}_\xi} B_{\epsilon_q}^\infty(\xi_q) \subseteq \mathcal{G}_s(\mathcal{D}). \quad (21)$$

In words, if $\xi_q \in \mathbb{R}^{(n+m)T}$ were safe, (20) computes the largest hypercube in $\mathbb{R}^{(n+m)T}$ that is centered at ξ_q and contained in $\mathcal{G}_s(\mathcal{D})$; if ξ_q were unsafe, then (20) returns zero. Moreover, one can inner approximate the guaranteed safe set $\mathcal{G}_s(\mathcal{D})$ by taking the union of the $B_{\epsilon_q}^\infty(\xi_q)$ hypercubes. For the proof of Thm. 2, see App. C.2.

To inner approximate the learned *unsafe* set $\mathcal{G}_{\gamma_s}(\mathcal{D})$, we replace (20b) with the condition that the trajectory ξ is safe, i.e., $\mathbf{g}_k(\xi, \theta) \leq 0$, and proceed as described in Thm. 2 above.

Alternatively, under some constraint parameterizations, the volume extraction problem is more naturally posed and easily

solved in parameter (θ) space than in trajectory (ξ) space, as is the case for the line-of-sight constraint (see Sec. V-C). In this alternative approach, formalized as Thm. 3 and detailed below, we iteratively reject parameter values in Θ that are incompatible with the interaction demonstrations in \mathcal{D} .

Theorem 3 (Volume Extraction Over Parameter Space): Given a set of queried parameters $\mathcal{Q}_\theta := \{\theta_q \in \Theta : q \in [Q_\theta]\}$, for each $\theta_q \in \mathcal{Q}_\theta$, define:

$$r_q := \min_{\theta \in \mathcal{F}(\mathcal{D})} \|\theta - \theta_q\|_\infty. \quad (22)$$

Then:

$$\bigcap_{\theta \in \mathcal{F}(\mathcal{D}) \setminus \bigcup_{q \in [Q_\theta]} B_{r_q}^\infty(\theta_q)} \{\xi \in \mathbb{R}^{(n+m)T} : \mathbf{g}(\xi, \theta) \leq 0\} = \mathcal{G}_s(\mathcal{D}). \quad (23)$$

In words, if a parameter value $\theta_q \in \mathcal{Q}_\theta$ were incompatible with the local Nash stationarity of \mathcal{D} (i.e., if $\theta_q \notin \mathcal{F}(\mathcal{D})$), then (22) characterizes the largest hypercube $B_{r_q}^\infty(\theta_q)$ in Θ , centered at θ_q , such that all $\theta \in B_{r_q}^\infty(\theta_q)$ are incompatible with the local Nash stationarity of \mathcal{D} . Otherwise, if $\theta_q \in \mathcal{F}(\mathcal{D})$, then (22) returns zero. Thus, the true parameter θ^* must lie outside of all hypercubes of side length $2r_q$ centered at θ_q , i.e., outside $\bigcup_{q \in [Q_\theta]} B_{r_q}^\infty(\theta_q)$. Finally, Thm. 3 states that the guaranteed safe set $\mathcal{G}_s(\mathcal{D})$ can be computed as the set of all trajectories marked safe by feasible parameters outside $\bigcup_{q \in [Q_\theta]} B_{r_q}^\infty(\theta_q)$. For the proof of Thm. 3, see App. C.2 [8].

Remark 3: In practice, to form \mathcal{Q}_ξ , one can sample safe trajectories from the vicinity of each demonstration trajectory in \mathcal{D} . To form \mathcal{Q}_θ , one can sample parameter values θ that characterize constraints under which some demonstration trajectory in \mathcal{D} would be unsafe.

The guaranteed unsafe set $\mathcal{G}_{\neg s}(\mathcal{D})$ can be similarly characterized via volume extraction over Θ . Since the extracted estimates of $\mathcal{G}_s(\mathcal{D})$ and $\mathcal{G}_{\neg s}(\mathcal{D})$ (termed $\hat{\mathcal{G}}_s(\mathcal{D})$ and $\hat{\mathcal{G}}_{\neg s}(\mathcal{D})$ below, respectively) either equal or inner approximate $\mathcal{G}_s(\mathcal{D})$ and $\mathcal{G}_{\neg s}(\mathcal{D})$, respectively, they can be *directly* used by a motion planner downstream to verify constraint satisfaction or violation. Concretely, any generated trajectory in $\hat{\mathcal{G}}_s(\mathcal{D})$ is guaranteed safe, while any trajectory outside $\hat{\mathcal{G}}_{\neg s}(\mathcal{D})$ is at least not guaranteed to be unsafe. Alternatively, a motion planner can design safe trajectories via *implicit* constraint checking, e.g., via Model Predictive Path Integral (MPPI) control [27], summarized as thus: We sample i.i.d. control sequences near a given nominal control sequence, and update our nominal controls to be a convex combination of the sampled controls, with weights computed using the cost and degree of constraint violation incurred along each corresponding state trajectory. For details, see App. D [8].

D. Theoretical Limitations of Constraint Learnability

Here, we present conditions under which the constraint parameter θ is provably irrecoverable, thus establishing theoretical limitations on constraint learnability (Thm. 4).

Theorem 4 (Limitations of Learnability): For any $\theta \in \Theta$, let $\mathcal{D}(\theta)$ denote the set of local Nash stationary trajectories

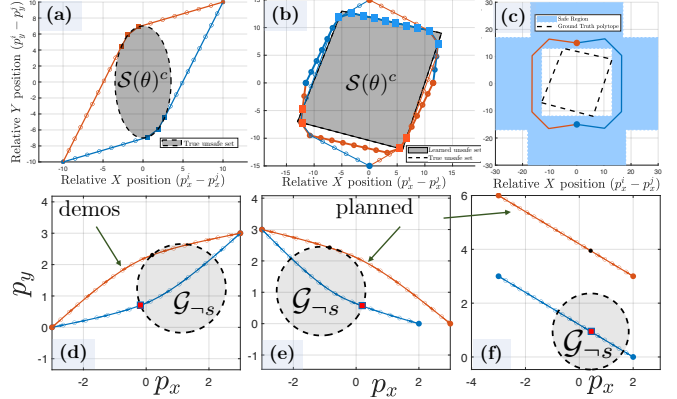


Fig. 2: Learned constraint sets of Agent 1 (blue) and 2 (orange) with double integrator dynamics and (a) ellipsoidal, (b) polytopic, or (d) velocity-dependent spherical collision avoidance constraints. (c) Inner approximation of the safe set (from (b)) via volume extraction, and corresponding safe motion plans. (e, f) Motion plans designed using learned constraints from (d). In all subplots, solid circles at the ends of the trajectories indicate start and goal positions. In (a) and (b), solid squares indicate tight (i.e., activated) constraints. In (d), (e), and (f), red (resp., black) squares indicate Agent 1 (resp., 2) states corresponding to the gray velocity-dependent spherical constraints depicted.

corresponding to the constraints $\mathbf{h}(\xi) = 0$, $\mathbf{g}_k(\xi) \leq 0$, and $\mathbf{g}_{\neg k}(\xi, \theta) \leq 0$, i.e.,:

$$\begin{aligned} \mathcal{D}(\theta) := \{\xi \in \mathbb{R}^{(n+m)T} : & \exists \lambda_k, \lambda_{\neg k}, \nu \\ & \text{s.t. } (\theta, \lambda_k, \lambda_{\neg k}, \nu) \in \text{KKT}(\{\xi\})\}. \end{aligned} \quad (24)$$

Suppose the constraint vector $\mathbf{g}_{\neg k}(\cdot, \cdot)$ can be partitioned into two components, $\mathbf{g}_{\neg k}^{(1)}(\cdot, \cdot)$ and $\mathbf{g}_{\neg k}^{(2)}(\cdot, \cdot)$, such that the constraint $\mathbf{g}_{\neg k}^{(2)}(\xi, \theta^*) \leq 0$ is strictly looser than the remaining constraints $\mathbf{h}(\xi) = 0$, $\mathbf{g}_k(\xi) \leq 0$, $\mathbf{g}_{\neg k}^{(1)}(\xi, \theta^*) \leq 0$, i.e.,:

$$\begin{aligned} \{\xi \in \mathbb{R}^{(n+m)T} : \mathbf{h}(\xi) = 0, \mathbf{g}_k(\xi) \leq 0, \mathbf{g}_{\neg k}^{(1)}(\xi, \theta^*) \leq 0\} \\ \subseteq \{\xi \in \mathbb{R}^{(n+m)T} : \mathbf{g}_{\neg k}^{(2)}(\xi, \theta^*) < 0\}. \end{aligned} \quad (25)$$

Then, for any parameter value θ satisfying:

$$\mathbf{g}_{\neg k}^{(1)}(\cdot, \theta^*) = \mathbf{g}_{\neg k}^{(1)}(\cdot, \theta), \quad (26)$$

$$\begin{aligned} \{\xi \in \mathbb{R}^{(n+m)T} : \mathbf{h}(\xi) = 0, \mathbf{g}_k(\xi) \leq 0, \mathbf{g}_{\neg k}^{(1)}(\xi, \theta^*) \leq 0\} \\ \subseteq \{\xi \in \mathbb{R}^{(n+m)T} : \mathbf{g}_{\neg k}^{(2)}(\xi, \theta) < 0\}, \end{aligned} \quad (27)$$

we have $\mathcal{D}(\theta^*) = \mathcal{D}(\theta)$.

In words, each local Nash stationary demonstration corresponding to θ^* is also at local Nash stationarity under θ , and vice versa. Thus, when inferring constraints from demonstrations, θ will always remain as a valid alternative to θ^* . The proof of Thm. 4, as well as a motivating example, are presented in App. C.3 [8].

V. EXPERIMENTS

To validate our methods, we perform constraint learning and volume extraction-based safe motion planning under elliptical and polytopic constraint parameterizations (Sec. V-A), via simulations on double integrator (Sec. V-B) and

quadcopter (Sec. V-D) dynamics, and hardware experiments on ground robots with unicycle dynamics (Sec. V-G). For each agent dynamics and constraint type, we solve (3) using a given set of costs J^i and ground truth constraints (via the KKT conditions (4)) to generate demonstrations \mathcal{D} that activate the unknown constraint. We solve (7a) to learn constraints in simulation and (12) to learn constraints from hardware demonstrations that may not satisfy the KKT conditions (4) perfectly. We also use the recovered constraints to generate safe motion plans; in contrast, a cost inference-based baseline method generates unsafe trajectories (Sec. V-H). Our experiments are implemented with YALMIP [28], Gurobi [25], CasADi [29], and IPOPT [30]. For additional experiments and details, see App. E [8].

A. Constraint Parameterizations and Agent Costs

In our experiments, we consider the following constraint parameterizations over agent states $\{x_t^i : i \in [N], t \in [T]\}$. We denote by p_t^i and v_t^i the components of x_t^i corresponding to position and velocity, respectively, $\forall i \in [N], t \in [T]$ ⁴.

a) *Elliptical Constraints*: We encode elliptical collision avoidance constraints for 2D systems via the parameterization $g_{i,\neg k}^i(\xi, \theta^i) = -(p_t^i - p_t^j)^\top \text{diag}\{\theta_2^i, \theta_3^i\}(p_t^i - p_t^j) + (\theta_1^i)^2 \leq 0$ with $\theta_k^i > 0, \forall k \in [3]$, where $\text{diag}\{\cdot\}$ describes a diagonal matrix with given entries as diagonal values⁵. As a special case, this parameterization encodes spherical collision avoidance constraints when $\theta_2^i = \theta_3^i = 1, \forall i \in [N]$ are known. Moreover, by replacing $(p_t^i - p_t^j)$ with $(p_t^i - p_t^j, v_t^i - v_t^j)$ and increasing the dimension of $\text{diag}\{\theta_2^i, \theta_3^i\}$, we encode *velocity-dependent* collision avoidance, which allows agents to modulate their collision avoidance radii depending on whether other agents are approaching or moving away.

b) *Polytopic Constraints*: We use intersections of unions of half-spaces to encode polytopic constraints for each agent $i \in [N]$ via the parameterization:

$$C_{\neg k}^{\text{ineq},i} = \bigwedge_{t \in [T]} \bigwedge_{j \in [N] \setminus \{i\}} \bigwedge_{\alpha \in [N_c]} \bigvee_{\beta \in [N_c]} \{A_{\alpha,\beta}(\theta)(p_t^j - p_t^i) \leq b_{\alpha,\beta}(\theta)\}.$$

where $A_{\alpha,\beta}(\theta)$ and $b_{\alpha,\beta}(\theta)$ are components of θ across indices α, β . As special cases, the above parameterization can encode polytopic collision avoidance and proximity constraints (which bound agents' relative positions). By replacing $A_{\alpha,\beta}(\theta)(p_t^j - p_t^i)$ with $A_{\alpha,\beta}(\theta)(p_t^j - p_t^i) + \bar{A}_{\alpha,\beta}(\theta)(v_t^j - v_t^i)$ above, we can encode line-of-sight constraints which compel agents to keep other agents in sight, an important requirement for pursuit-evasion or herding applications [31].

c) *Origin and Goal Constraints*: In all experiments, the trajectory of each agent $i \in [N]$ is constrained by a prescribed set of origin (\bar{p}_o^i) and goal (\bar{p}_d^i) positions, enforced via the (known) constraint $h_t^i(\xi) := (p_0^i - \bar{p}_o^i, p_T^i - \bar{p}_d^i) = 0$.

⁴We show in App. E [8] that many dynamics models which do not explicitly encode the system's velocity in the state, e.g., 2D unicycles, can be transformed into equivalent dynamics models that do.

⁵For 3D systems, we replace $\text{diag}\{\theta_2^i, \theta_3^i\}$ with $\text{diag}\{\theta_2^i, \theta_3^i, \theta_4^i\}$

d) *Agent Costs*: Unless otherwise specified, each agent's cost is the individual smoothness cost $J^i := \sum_{t=1}^{T-1} \|p_{t+1}^i - p_t^i\|_2^2$, or shared smoothness cost $J^i := \sum_{t=1}^{T-1} \sum_{j=1}^N \|p_{t+1}^j - p_t^j\|_2^2$.

B. Double Integrator Simulations

a) *Constraint Inference*: We validate our method by recovering polytopic, elliptic, and velocity-dependent spherical collision avoidance constraints. Fig. 2a-2b plot demonstrations generated via solving (3) across all $i \in [N]$, and mark timesteps when constraints are active. By solving (7), we were able to recover the true constraint parameter θ^* .

b) *Motion Planning*: To evaluate our volume extraction approach for planning (Sec. IV-C and App. D) [8], we generate safe trajectories which satisfy a given set of polytopic collision-avoidance constraints. Concretely, using a set of queried trajectories \mathcal{Q}_ξ , we extract hypercubes of safe trajectories which were then used for constraint checking during trajectory generation. Our method generates constraint-satisfying trajectories for each agent (Fig. 2d). Moreover, Fig. 10 in App. E.4 [8] presents MPPI-generated robust motion plans, informed by safe trajectories queried via volume extraction methods, that are safe with respect to an underlying constraint that is conservatively but not perfectly recovered. In contrast, naive motion plans designed using a point estimate of the constraint parameter are unsafe.

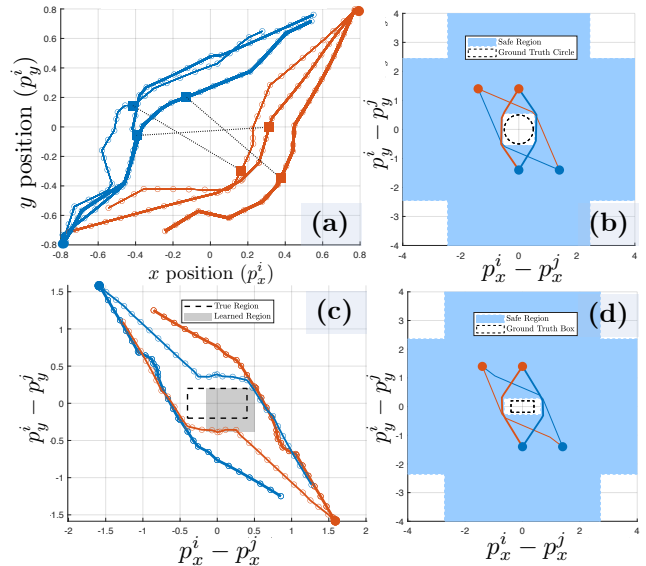


Fig. 3: (a) Demonstrations (delimited by linewidth) and (b) safe planning via volume extraction for hardware unicycle agents 1 (blue) and 2 (orange) with spherical collision-avoidance constraints. (c)-(d) present the box-constraint case; despite reduced recovery accuracy from demonstrator sub-optimality, the volume-extraction planner still produces safe trajectories. In (a), squares on and dashed lines between trajectories indicate constraint activation (i.e., tightness).

c) *Compute Time vs. Number of Agents*: For the inference of spherical collision avoidance constraints between agents with double integrator dynamics, we record Gurobi solve times for problem instances with different numbers of

agents N . The $N = 2, 10, 20, 30, 100$ settings respectively required 0.03 s, 0.16 s, 0.22 s, 2.87 s, and 6.24 s to solve, indicating that our method remains tractable on large-scale problems. Similarly, the $N = 2, 4, 10$ instances for box collision avoidance constraints required 0.06 s, 0.59 s, and 5.37 s to solve, respectively. For details, see App. E [8].

C. Unicycle Simulations

In simulations of interacting agents with unicycle dynamics, our method recovers unknown line-of-sight and spherical proximity and collision avoidance constraints from local Nash interactions (Fig. 4a and 4c). We then used volume extraction (Sec. IV-C) to compute safe interactive motion plans (Fig. 4b and 4d). For details, see App. E.5 [8].

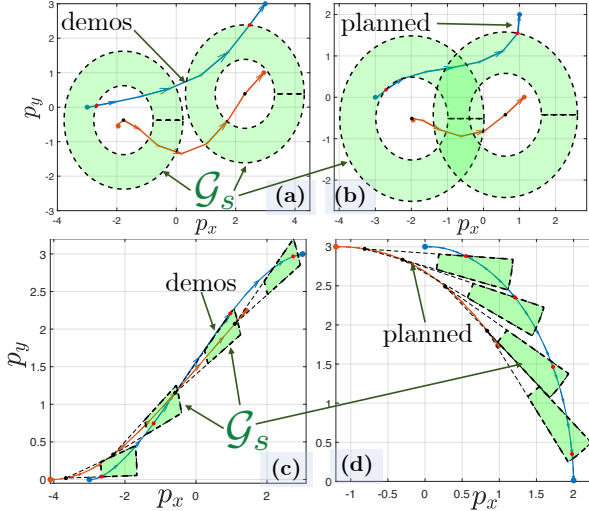


Fig. 4: Constraint learning and planning for Agent 1 (blue) and 2 (orange) with unicycle dynamics satisfying (a, b) proximity or (c, d) line of sight. Learned constraints (shaded green) coincide with the true constraints (dashed black lines).

D. Quadcopter Simulations

We accurately recover spherical (Fig. 5) and box-shaped (App. E.6 [8], Fig. 14) collision avoidance constraints from interaction demonstrations at local Nash stationarity between 3 agents with 12-D quadcopter dynamics. We then compute safe motion plans via volume extraction. In contrast, the baseline single-agent constraint learning method in [1], which treats Agents 1 and 3 as unconstrained moving obstacles, failed to recover the constraint of Agent 2 and incorrectly perceived the provided demonstrations as suboptimal, with a stationarity error of 1.8. For details, see App. E.6 [8].

E. Nonlinear Constraint Recovery under Cost Uncertainty

Our method can learn constraints and generate safe plans even when the agents' objectives are also *a priori* unknown, or when the constraint parameterization is nonlinear in agent states, leading to nonconvex unsafe sets. For illustration, we simulate two interacting agents with single integrator dynamics. Relevant figures are in App. E.7 [8].

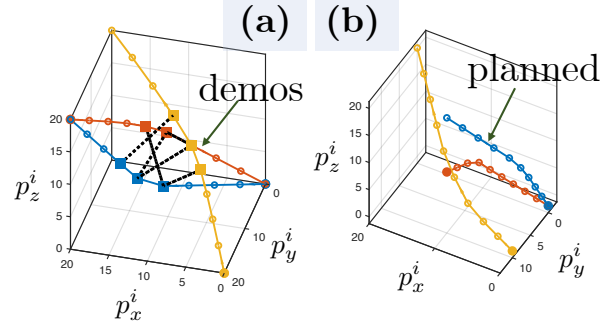


Fig. 5: Constraint learning and planning for Agents 1 (blue), 2 (orange), and 3 (yellow) with quadcopter dynamics satisfying spherical collision-avoidance constraints. (a) A demonstration of all agents, in absolute coordinates, interacting while satisfying the constraints. Our method exactly learns all constraint parameters. Filled squares on, and dashed lines between, trajectories indicate tight constraints. (b) Using our learned constraints, we generate safe motion plans via volume extraction over the trajectory space.

F. Learning with Misspecified Constraint Parameterizations

We simulate a constraint learner who mistakenly believes that the ellipse-shaped collision-avoidance constraint underlying an interaction demonstration is a union of box-shaped constraints (Fig. 6). Despite this incorrect belief, our method still reasonably approximated the ellipse-shaped collision avoidance constraint as the union of three boxes with zero stationarity. This result illustrates that given a constraint parameterization, the number of constraint sets recovered can be flexibly adjusted to explain the demonstration's optimality.

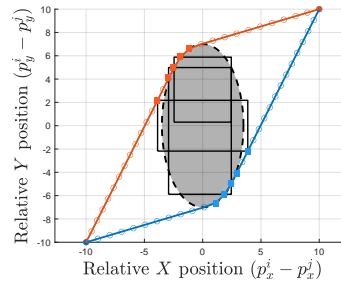


Fig. 6: Our method well-approximates an ellipsoidal collision-avoidance set as the union of three boxes from interaction demonstrations with bicycle dynamics, even when constraints are mistakenly assumed to be box-parameterized.

G. Hardware Experiments

We demonstrate constraint inference and safe motion planning on hardware experiments involving two agents with unicycle dynamics whose trajectories satisfy spherical or box-shaped collision-avoidance or line-of-sight (Fig. 3 and Fig. 1 time-lapses) constraints. Despite suboptimality in the hardware demonstrations, our volume extraction-based motion planning method inner approximated the guaranteed safe set, and generated safe trajectories for both agents.

H. Comparison Against Cost Inference Baseline

Finally, we compare the efficacy of our constraint learning-based method for safe motion planning against the cost inference-based approach in [4]. Specifically, we simulate interacting agents with double integrator dynamics who abide

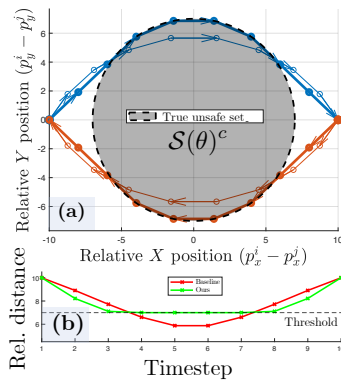


Fig. 7: (a) Local Nash trajectories of Agents 1 (blue) and 2 (orange) in relative coordinates, using spherical constraints learned via our method (thick) and the baseline [4] (thin, Sec. V-H). Baseline trajectories overlap the circular unsafe set, with violations further shown in the inter-agent distance-time plot in (b).

by *a priori* unknown spherical collision avoidance constraints. Our method recovers the constraints, which are then used for motion planning via solving the KKT conditions (4) for the forward game (3). Meanwhile, the approach in [4] assumes each agent i 's collision avoidance intent is embedded in its cost $\tilde{J}^i(\tilde{\theta})$ as a log barrier with an unknown weight $\tilde{\theta}$, i.e., $\tilde{J}^i(\tilde{\theta}) := J^i - \tilde{\theta} \cdot \sum_{t=1}^T \log(\|p_t^i - p_t^{2-i}\|_2^2)$. Then, the method in [4] infers $\tilde{\theta}$ from data, and uses $\tilde{J}^i(\theta)$ to design motion plans by solving the forward dynamic game (3) *without explicit constraints*. Fig. 7 shows that, while our method generates safe plans, the approach in [4] produces constraint-violating plans. Across 100 demonstrations with distinct initial and goal positions, our method required an average runtime of 99.4 ± 11.2 ms and always generated constraint-abiding interactions, while the method in [4] required an average runtime of 68.7 ± 39.8 ms⁶ but generated constraint-violating plans 36% of the time.

VI. CONCLUSION AND FUTURE WORK

We presented an inverse dynamic games-based constraint learning framework that infers strategic agents' coupled constraints from demonstrations of their equilibrium interactions, and uses the inferred constraints for robust, safe motion planning. In simulation and hardware experiments, our method accurately infers agent constraints and generates robust motion plans, even when using demonstrations away from local Nash equilibria. Future work will extend our approach to infer temporally-extended interaction constraints [32], and infer interaction constraints with unknown parameterization using Gaussian processes [11].

REFERENCES

- [1] G. Chou, N. Ozay, and D. Berenson, "Learning Constraints From Locally-Optimal Demonstrations Under Cost Function Uncertainty," *IEEE RA-L*, vol. 5, no. 2, 2020.
- [2] —, "Learning Parametric Constraints in High Dimensions from Demonstrations," in *CoRL*, 2020.
- [3] D. McPherson, K. Stocking, and S. Sastry, "Maximum Likelihood Constraint Inference from Stochastic Demonstrations," in *CCTA*, 2021.
- [4] L. Peters, D. Fridovich-Keil, V. Rubies-Royo, C. J. Tomlin, and C. Stachniss, "Inferring Objectives in Continuous Dynamic Games from Noise-Corrupted Partial State Observations," in *RSS*, 2021.
- [5] J. Li, C.-Y. Chiu, L. Peters, S. Sojoudi, C. Tomlin, and D. Fridovich-Keil, "Cost Inference for Feedback Dynamic Games from Noisy Partial State Observations and Incomplete Trajectories," in *AAMAS*, 2023.
- [6] N. Mehr, M. Wang, M. Bhatt, and M. Schwager, "Maximum-entropy multi-agent dynamic games: Forward and inverse solutions," *IEEE T-RO*, vol. 39, no. 3, 2023.
- [7] S. Le Cleac'h, M. Schwager, and Z. Manchester, "LUCIDGames: Online Unscented Inverse Dynamic Games for Adaptive Trajectory Prediction and Planning," *IEEE RA-L*, 2021.
- [8] Anonymous, "Constraint Learning in Multi-Agent Dynamic Games from Demonstrations of Local Nash Interactions (Extended)," 2025. [Online]. Available: <https://drive.google.com/file/d/1FnH97fJpqCuYH776f6WXIvfq7OOUdu3KS/view>
- [9] P. Englert, N. Vien, and M. Toussaint, "Inverse KKT: Learning Cost Functions of Manipulation Tasks from Demonstrations," *IJRR*, 2017.
- [10] M. Menner, P. Worsnop, and M. N. Zeilinger, "Constrained Inverse Optimal Control With Application to a Human Manipulation Task," *IEEE TCST*, 2021.
- [11] G. Chou, H. Wang, and D. Berenson, "Gaussian Process Constraint Learning for Scalable Chance-Constrained Motion Planning From Demonstrations," *IEEE RA-L*, vol. 7, no. 2, pp. 3827–3834, 2022.
- [12] N. Mehr, R. Horowitz, and A. D. Dragan, "Inferring and Assisting with Constraints in Shared Autonomy," in *IEEE CDC*, 2016.
- [13] C. Li and D. Berenson, "Learning Object Orientation Constraints and Guiding Constraints for Narrow Passages from One Demonstration," in *ISER*, 2016.
- [14] S. Calinon and A. Billard, "A Probabilistic Programming by Demonstration Framework Handling Constraints in Joint Space and Task Space," in *IROS*, 2008.
- [15] T. Başar and G. Olsder, *Dynamic Noncooperative Game Theory*. Society for Industrial and Applied Mathematics, 1998.
- [16] B. Di and A. Lamperski, "Newton's Method and Differential Dynamic Programming for Unconstrained Nonlinear Dynamic Games," in *CDC*, 2019.
- [17] D. Fridovich-Keil, E. Ratner, L. Peters, A. Dragan, and C. J. Tomlin, "Efficient Iterative Linear-Quadratic Approximations for Nonlinear Multi-Player General-Sum Differential Games," *ICRA*, 2020.
- [18] S. Le Cleac'h, M. Schwager, and Z. Manchester, "ALGAMES: a Fast Augmented Lagrangian Solver for Constrained Dynamic Games," *Auton. Robots*, 2022.
- [19] T. Kavuncu, A. Yaraneri, and N. Mehr, "Potential iLQR: A Potential-Minimizing Controller for Planning Multi-Agent Interactive Trajectories," *RSS*, 07 2021.
- [20] C. Awasthi and A. Lamperski, "Inverse differential games with mixed inequality constraints," in *ACC*, 2020.
- [21] H. I. Khan and D. Fridovich-Keil, "Leadership Inference for Multi-Agent Interactions," *IEEE Robotics and Automation Letters*, vol. 9, no. 5, pp. 4671–4678, 2024.
- [22] C. Armstrong, R. Park, X. Liu, K. Gupta, and D. Fridovich-Keil, "Inferring Foresightedness in Dynamic Noncooperative Games," *IEEE Robotics and Automation Letters*, vol. 10, no. 12, 2025.
- [23] L. Peters, A. Bajcsy, C.-Y. Chiu, D. Fridovich-Keil, F. Laine, L. Ferriani, and J. Alonso-Mora, "Contingency Games for Multi-Agent Interaction," *IEEE RA-L*, vol. 9, no. 3, pp. 2208–2215, 2024.
- [24] X. Liu, L. Peters, J. Alonso-Mora, U. Topcu, and D. Fridovich-Keil, "Auto-Encoding Bayesian Inverse Games," *WAFR*, 2024.
- [25] Gurobi Optimization, LLC, "Gurobi Optimizer Reference Manual," 2024. [Online]. Available: <https://www.gurobi.com>
- [26] D. Bertsimas and J. Tsitsiklis, *Introduction to Linear Optimization*. Athena Scientific, 01 1998.
- [27] G. Williams, P. Drews, B. Goldfain, J. Rehg, and E. Theodorou, "Aggressive Driving with Model Predictive Path Integral Control," in *ICRA*, 2016.
- [28] J. Löfberg, "YALMIP : A Toolbox for Modeling and Optimization in MATLAB," in *CACSD*, 2004.
- [29] J. A. E. Andersson, J. Gillis, G. Horn, J. B. Rawlings, and M. Diehl, "CasADi: A Software Framework for Nonlinear Optimization and Optimal Control," *Mathematical Programming Computation*, 2019.
- [30] A. Wächter and L. T. Biegler, "On the Implementation of an Interior-point Filter Line-search Algorithm for Large-scale Nonlinear Programming," *Mathematical Programming*, vol. 106, pp. 25–57, 2006.
- [31] Z. Zhou, W. Zhang, J. Ding, H. Huang, D. M. Stipanović, and C. J. Tomlin, "Cooperative Pursuit with Voronoi Partitions," *Automatica*, vol. 72, pp. 64–72, 2016.
- [32] M. Vazquez-Chanlatte, S. Jha, A. Tiwari, M. Ho, and S. Seshia, "Learning Task Specifications from Demonstrations," in *NeurIPS*, 2018.

⁶Since the approach in [4] can be posed as an optimization problem with no binary variable, it is, unsurprisingly, slightly faster than our method.

APPENDIX

Below, App. A presents a table of commonly used notation in our work. App. B then illustrates how the constraint recovery problem (7) can be recast as a mixed-integer linear program (MILP) for offset-parameterized constraints. Next, App. C presents proofs of theoretical results presented in the main paper and establishes additional theoretical results beyond those given in the main paper. Then, App. D describes the implicit constraint checking-based safe trajectory design first described at the end of Sec. IV-C. Finally, App. E provide additional details for the experiments whose results are described in Sec. V.

A. Table of Notation

TABLE I: Notation commonly used throughout the work.

Symbol	Definition
N	Number of agents
T	Time horizon length
x_t^i	State of agent $i \in [N]$ at time $t \in [T]$
u_t^i	Control of agent $i \in [N]$ at time $t \in [T]$
x_t	State at time $t \in [T]$, i.e., $x_t := (x_t^1, \dots, x_t^N)$
u_t	Control at time $t \in [T]$, i.e., $u_t := (u_t^1, \dots, u_t^N)$
x	System-level state trajectory, i.e., $x := (x_1, \dots, x_T)$
u	System-level control trajectory, i.e., $u := (u_1, \dots, u_T)$
$J^i(\xi)$	Cost function of agent $i \in [N]$
$h_\beta^i(\xi) = 0$	β -th ($\beta \in [N]^{eq,i}$) equality constraint of agent $i \in [N]$ across all times
$g_{\beta,k}^i(\xi) \leq 0$	β -th ($\beta \in [N]^{ineq,i}$) known inequality constraint of agent $i \in [N]$ across all times
$g_{\beta,\neg k}^i(\xi, \theta) \leq 0$	β -th ($\beta \in [N]_{\neg k}^{ineq,i}$) unknown inequality constraint of agent $i \in [N]$ across all times
θ^*	True unknown constraint parameter
Θ	Parameter space, i.e., the set of all possible parameter values (Note: $\theta^* \in \Theta$)
$\mathbf{h}^i, \mathbf{g}_k^i, \mathbf{g}_{\neg k}^i$	Stacked equality, known inequality, and unknown inequality constraints for agent $i \in [N]$
$\mathbf{h}, \mathbf{g}_k, \mathbf{g}_{\neg k}$	Stacked equality, known inequality, and unknown inequality constraints across all agents
$\mathcal{S}(\theta)$	Safe set, i.e., the set of all safe trajectories $\{\xi : \mathbf{g}_{\neg k}^i(\xi, \theta) \leq 0\}$
$\mathcal{A}(\theta)$	Unsafe set, given by $\mathcal{A}(\theta) = \mathcal{S}(\theta)^c$
$\mathcal{D} = \{\xi_d^{\text{loc}}\}_{d=1}^D$	Dataset of locally Nash-stationary demonstrations
$\lambda_{d,k}^i$	Lagrange multipliers for known inequalities for agent $i \in [N]$ in demonstration $d \in [D]$
$\lambda_{d,\neg k}^i$	Lagrange multipliers for unknown inequalities for agent $i \in [N]$ in demonstration $d \in [D]$
ν_d^i	Lagrange multipliers for equalities for agent $i \in [N]$ w.r.t. the demonstration $d \in [D]$
$\lambda_k, \lambda_{\neg k}, \nu$	$\lambda_{d,k}^i, \lambda_{d,\neg k}^i$, and ν_d^i stacked across all agents and demonstrations, respectively
$\nabla_x \mathbf{f}$	Jacobian of \mathbf{f}
$\text{stat}^i(\xi_d^{\text{loc}})$	KKT stationarity residual term corresponding to agent $i \in [N]$ and demonstration $d \in [D]$
$\text{KKT}^i(\xi_d^{\text{loc}})$	KKT-feasible set of parameters θ and Lagrange multipliers $(\lambda_k, \lambda_{\neg k}, \nu)$ w.r.t. agent $i \in [N]$ and the demonstration ξ_d^{loc}
$\text{KKT}(\mathcal{D})$	Intersection of $\text{KKT}^i(\xi_d^{\text{loc}})$ across all agents and demonstrations in \mathcal{D}
$\mathcal{F}(\mathcal{D})$	Parameters in Θ consistent with demonstrations in \mathcal{D}
$\mathcal{G}_s(\mathcal{D})$	Guaranteed safe trajectories w.r.t. all $\theta \in \mathcal{F}(\mathcal{D})$
$\mathcal{G}_{\neg s}(\mathcal{D})$	Guaranteed unsafe trajectories w.r.t. all $\theta \in \mathcal{F}(\mathcal{D})$

B. MILPs for Inferring Polytopic Constraints

In this subsection, we elaborate on how the constraint recovery problem (7) can be formulated as a mixed-integer linear program (MILP) B.1 for offset-parameterized constraints. We also discuss how (7) can be formulated as a mixed-integer bilinear program (MIBLP) in B.2 for affine-parameterized constraints.

In Sections B.1 and B.2 below, we use the following notation: Given any trajectory $\xi \in \mathbb{R}^{(n+m)T}$, let $x_t^i(\xi) \in \mathbb{R}^{n_i}$ denote the value of agent i 's state at time t , as prescribed by the trajectory ξ . We also define $u_t^i(\xi) \in \mathbb{R}^{m_i}$, $x_t(\xi) \in \mathbb{R}^n$, and $u_t(\xi) \in \mathbb{R}^m$ similarly.

1) *Reformulation of the Constraint Inference Problem for Unions of Offset-Parameterized Constraints*: Below, we present a more detailed explanation of the fact, first introduced in Sec. IV-B, the problem of learning *offset-parameterized interaction constraints* in the context of dynamic games can be reformulated as MILPs. We note that offset-parameterized interaction constraints often arise in dynamic games, e.g., in the context of spherical or box-shaped collision-avoidance constraints with uncertain dimensions. In particular, consider the specific setting in which the states of each agent have equal dimension (i.e., $n_i = n_j$ for each $i, j \in [N]$). the unknown constraints $\mathbf{g}_{\neg k}^i(\xi, \theta) \leq 0$ encode that for all $t \in [T]$, the state of each other agent $j \in [N] \setminus \{i\}$ relative to agent i lies outside a polytopic collision avoidance set with N_c sides, each of which can be represented as a scalar constraint. Concretely, feasible system-level trajectories must lie outside the avoid sets:

$$\mathcal{A}^{i,j,t}(\theta) := \bigcap_{\beta=1}^{N_c} \{\xi \in \mathbb{R}^{(n+m)T} : \mathbf{a}_\beta^{i,j,t\top} \xi < b_\beta^i(\theta)\} \quad (28)$$

for all $i, j \in [N], j \neq i$ and $t \in [T]$, where, for each $\beta \in [N_c]$, the vector $\mathbf{a}_\beta^{i,j,t} \in \mathbb{R}^{(n+m)T}$ and the scalar $b_\beta^i(\theta) \in \mathbb{R}$ for each $i, j \in [N], j \neq i$ $t \in [T]$ together represent one of the N_c sides of the polytope-shaped collision-avoidance constraint set. Moreover, each $b_\beta^i(\theta) \in \mathbb{R}$ is specified by an unknown parameter θ . Thus, the trajectory ξ must evade the avoid set $\mathcal{A}(\theta) \subset \mathbb{R}^{(n+m)T}$, given by:

$$\mathcal{A}(\theta) := \bigcup_{i,j \in [N], j \neq i, t \in [T]} \mathcal{A}^{i,j,t}(\theta), \quad (29)$$

or equivalently, stay within the safe set $\mathcal{S}(\theta) := (\mathcal{A}(\theta))^c \subset \mathbb{R}^{(n+m)T}$ given by:

$$\mathcal{S}(\theta) := \bigcap_{i,j \in [N], j \neq i, t \in [T]} \bigcup_{\beta \in [N_c]} \{\xi : \mathbf{a}_\beta^{i,j,t\top} \xi \geq b_\beta^i(\theta)\}$$

We now present a transformation of the primal feasibility conditions (4a), complementary slackness conditions (4c)-(4c), and stationarity conditions (4d) that allow us to reformulate the KKT conditions (7) into an MILP. Our method extends the approach presented in Sections IV-B of [1] to accommodate the multi-agent constraint learning problem presented in this work.

1) **Reformulating the primal feasibility conditions (4a):**

First, we rewrite the primal feasibility conditions (4a) via the big-M formulation [1], [26] by introducing binary vectors $\mathbf{z}_d^{i,j,t} = (z_{d,\beta}^{i,j,t} \in \{0, 1\}) \in \{0, 1\}^{N_c}$ as shown below— $\forall d \in [D], i, j \in [N], t \in [T]$:

$$\begin{aligned} (\mathbf{A}^{i,j,t})^\top \xi_d^{\text{loc}} &\geq \mathbf{b}^i(\theta) - M(\mathbf{1}_{N_c} - \mathbf{z}_d^{i,j,t}), \quad (30a) \\ \sum_{\beta=1}^{N_c} z_{d,\beta}^{i,j,t} &\geq 1, \end{aligned}$$

Above, $M \gg 0$, $\mathbf{1}_{N_c} := (1, \dots, 1) \in \mathbb{R}^{N_c}$, while $\mathbf{A}^{i,j,t} \in \mathbb{R}^{(n+m)T \times N_c}$ and $\mathbf{b}^i(\theta) \in \mathbb{R}^{N_c}$ are the concatenations of $\mathbf{a}_\beta^{i,j,t}$ and $b_\beta^i(\theta)$, respectively, across all $\beta \in [N_c]$.

2) **Reformulating the complementary slackness conditions (4c):**

Let $\lambda_{d,\gamma_k}^{i,j,t} = (\lambda_{d,\beta,\gamma_k}^{i,j,t} \geq 0 : \beta \in [N_c]) \in \mathbb{R}^{N_c}$ denote the dual variables associated with the scalar inequality constraints $(\mathbf{a}_\beta^{i,j,t})^\top \xi \geq b_\beta^i(\theta)$, across $\beta \in [N_c]$. Since the safe set definition (15) involves a union over $\beta \in [N_c]$ for each $i, j \in [N], j \neq i, t \in [T]$, the constraint $\{\xi \in \mathbb{R}^{(n+m)T} : (\mathbf{a}_\beta^{i,j,t})^\top \xi^{\text{loc}} \geq b_\beta^i(\theta)\}$ might only be enforced for a strict (but non-empty) subset of the indices $\beta \in [N_c]$, which we denote by $B^{i,j,t} \subseteq [N_c]$. Likewise, complementary slackness (4c) should only be enforced for indices $\beta \in B^{i,j,t}$, for each $i, j \in [N], j \neq i, t \in [T]$, and in turn, terms of the form $\lambda_{d,\beta,\gamma_k}^{i,j,t} \nabla_{\xi^i} g_{\beta,\gamma_k}(\xi, \theta)$ are only included in the stationarity condition (4d) if $\beta \in B^{i,j,t}$. Thus, we use a big-M formulation with binary vectors $\hat{z}_{d,1}^{i,j,t} = (\hat{z}_{d,1,\beta}^{i,j,t} : \beta \in [N_c]) \in \{0, 1\}^{N_c}$ and $\hat{z}_{d,2}^{i,j,t} = (\hat{z}_{d,2,\beta}^{i,j,t} : \beta \in [N_c]) \in \{0, 1\}^{N_c}$ to encode (4c), and the binary vectors $\mathbf{q}_d^{i,j,t} = (q_{d,\beta}^{i,j,t} : \beta \in [N_c]) \in \{0, 1\}^{N_c}$ to encode enforcement of (4c). Then, we rewrite the complementary slackness conditions (4c) as follows— $\forall d \in [D], i, j \in [N], i \neq j, t \in [T]$:

$$\begin{bmatrix} \lambda_{d,\gamma_k}^{i,j,t} \\ \mathbf{A}^{i,j,t} \xi_d^{\text{loc}} - \mathbf{b}^i(\theta) \end{bmatrix} \leq M \begin{bmatrix} \hat{z}_{d,1}^{i,j,t} \\ \hat{z}_{d,2}^{i,j,t} \end{bmatrix}, \quad (31a)$$

$$\hat{z}_{d,1,\beta}^{i,j,t} + \hat{z}_{d,2,\beta}^{i,j,t} \leq 2 - q_{d,\beta}^{i,j,t}, \quad \forall \beta \in [N_c], \quad (31b)$$

$$\sum_{\beta'=1}^{N_c} q_{d,\beta'}^{i,j,t} \geq 1.$$

3) **Reformulating the stationarity condition (4d):**

As noted above, the stationarity condition (4d) includes the term $\lambda_{d,\beta,\gamma_k}^{i,j,t} \nabla_{\xi^i} g_{\beta,\gamma_k}(\xi, \theta)$ only if $\beta \in B^{i,j,t}$. To enforce this condition, for each $d \in [D], t \in [T], i, j \in [N], j \neq i$, we define $L_d^{i,j,t} \in \mathbb{R}^{N_c \times (n_i + m_i)T}$ as the matrix whose β -th row equals:

$$\lambda_{d,\beta,\gamma_k}^{i,j,t} \nabla_{\xi^i} (b_\beta^i(\theta) - \mathbf{a}_\beta^{i,j,t} \xi)^\top |_{\xi=\xi_d^{\text{loc}}}.$$

We then rewrite the term $\lambda_{d,\gamma_k}^{i,j,t} \nabla_{\xi^i} g_{\gamma_k}(\xi, \theta)$ in (4d) as follows— $\forall i \in [N], d \in [D], t \in [T]$:

$$\begin{aligned} &\sum_{j \in [N]} \sum_{t \in [T]} \lambda_{d,\gamma_k}^{i,j,t} \nabla_{\xi^i} (b^i(\theta) - \mathbf{A}^{i,j,t} \xi) |_{\xi=\xi_d^{\text{loc}}} \\ &= \sum_{j \in [N]} \sum_{t \in [T]} \mathbf{q}_d^{i,j,t} L_d^{i,j,t}. \end{aligned}$$

By replacing the bilinear terms $\mathbf{q}_d^{i,j,t} L_d^{i,j,t}$ in (18) with slack variables and adding constraints, we can reformulate (18) in a linear manner as well. Specifically, we define $\tilde{q}_d^{i,j,t} := 1 - q_d^{i,j,t}$ for each $d \in [D], i, j \in [N], j \neq i, t \in [T]$, and we introduce slack variables $R_d^{i,j,t} \in \mathbb{R}^{N_c \times (n_i + m_i)}$, for each $d \in [D], i, j \in [N], j \neq i, t \in [T]$. Let $R_{d,\beta,\ell}^{i,j,t}$ and $L_{d,\beta,\ell}^{i,j,t}$ respectively denote the β -th row and ℓ -th column entry of $R_d^{i,j,t}$ and $L_d^{i,j,t}$, for each $\beta \in [N_c], \ell \in [n]$. We assume that the slack variables $L_{d,\beta,\ell}^{i,j,t}$ are uniformly bounded below and above by \underline{M} and \bar{M} , respectively, across all indices $i, j \in [N], i \neq j, t \in [T], d \in [D], \beta \in [N_c], \ell \in [n_i + m_i]$. We then introduce the additional constraints below, for each $\beta \in [N_c]$ and $\ell \in [n]$, to linearize the bilinear terms of the form $\mathbf{q}_d^{i,j,t} L_d^{i,j,t}$:

$$\min\{0, \underline{M}\} \leq R_{d,\beta,\ell}^{i,j,t} \leq \bar{M}, \quad (32a)$$

$$\underline{M} q_{d,\beta}^{i,j,t} \leq R_{d,\beta,\ell}^{i,j,t} \leq \bar{M} q_{d,\beta}^{i,j,t}, \quad (32b)$$

$$L_{d,\beta,\ell}^{i,j,t} - \tilde{q}_{d,\beta}^{i,j,t} \bar{M} \leq R_{d,\beta,\ell}^{i,j,t} \quad (32c)$$

$$\leq L_{d,\beta,\ell}^{i,j,t} - \tilde{q}_{d,\beta}^{i,j,t} \underline{M}$$

$$R_{d,\beta,\ell}^{i,j,t} \leq L_{d,\beta,\ell}^{i,j,t} + \tilde{q}_{d,\beta}^{i,j,t} \bar{M} \quad (32d)$$

We now use (30), (31), and (32) to reformulate the constraint recovery problem (7) as follows:

$$\begin{aligned} \text{find} \quad &\theta, \lambda_{d,k}^{i,j,t}, \lambda_{d,\gamma_k}^{i,j,t}, \nu_d^i, R_d^{i,j,t}, L_d^{i,j,t}, \mathbf{q}_d^{i,j,t}, \tilde{q}_d^{i,j,t}, \\ &\mathbf{z}_{d,1}^{i,j,t}, \mathbf{z}_{d,2}^{i,j,t}, \quad \forall d, i, j, t \end{aligned} \quad (33a)$$

$$\begin{aligned} \text{s.t.} \quad &\text{Eqn. (30),} \quad \forall d \in [D], i, j \in [N] \\ &\text{s.t. } j \neq i, t \in [T], \end{aligned} \quad (33b)$$

$$\begin{aligned} &\lambda_{d,k}^{i,j,t}, \lambda_{d,\gamma_k}^{i,j,t} \geq 0, \quad \forall d \in [D], i, j \in [N] \\ &\text{s.t. } j \neq i, t \in [T], \end{aligned} \quad (33c)$$

$$\begin{aligned} &\text{Eqn. (31),} \quad \forall d \in [D], i, j \in [N] \\ &\text{s.t. } j \neq i, t \in [T], \end{aligned} \quad (33d)$$

$$\begin{aligned} &\nabla_{\xi^i} J^i(\xi_d^{\text{loc}}) + (\lambda_{d,k}^i)^\top \nabla_{\xi^i} \mathbf{g}_k^i(\xi_d^{\text{loc}}) \\ &+ \sum_{j \in [N]} \sum_{t \in [T]} \mathbf{1}_{N_c}^\top R_d^{i,j,t} \\ &+ (\nu_d^i)^\top \nabla_{\xi^i} \mathbf{h}^i(\xi_d^{\text{loc}}) = 0, \end{aligned} \quad (33e)$$

$$\forall d \in [D], i, j \in [N] \text{ s.t. } j \neq i, t \in [T],$$

$$\begin{aligned} &\text{Eqn. (32),} \quad \forall d \in [D], \beta \in [N_c], i, j \in [N] \\ &\text{s.t. } j \neq i, t \in [T], \end{aligned} \quad (33f)$$

where (33b) encodes primal feasibility, (33c) encodes the non-negativity of all Lagrange multiplier terms associated with inequality constraints, (33d)-(33e) encode complementary slackness, and (33f) encodes stationarity. We observe that (33) is indeed an MILP.

2) **Reformulation of the Constraint Inference Problem for Unions of Affine-Parameterized Constraints:** Below, we generalize the constraints (28) and (29) to accommodate the setting of *affine-parameterized* constraints, i.e., the setting in which the vectors $\mathbf{a}_\beta^{i,j,t} \in \mathbb{R}^n$, which are multiplied to the trajectories $\xi \in \mathbb{R}^{(n+m)T}$, are also *a priori* unknown and parameterized by the (unknown) constraint parameter θ .

Concretely, we assume that each agent $i \in [N]$ wishes to stay outside the following avoid sets, for each $j \in [N] \setminus \{i\}$, $t \in [T]$:

$$\mathcal{A}^{i,j,t}(\theta^*) := \bigcap_{\beta=1}^{N_c} \{\xi \in \mathbb{R}^{(n+m)T} : \mathbf{a}_\beta^{i,j,t}(\theta^*)^\top x < b_\beta^i(\theta^*)\}. \quad (34)$$

In other words, across all agents $i \in [N]$, the constraints $\mathbf{g}_{\gamma_k}^i(\xi, \theta^*) \leq 0$ together enforce that the trajectory ξ must avoid the following unsafe set:

$$\mathcal{A}(\theta^*) := \bigcup_{i,j \in [N], j \neq i, t \in [T]} \mathcal{A}^{i,j,t}(\theta^*). \quad (35)$$

If $N_c > 1$, one can rewrite the multiple constraints over which we are taking the intersection with a single constraint using the max operator. Thus, for ease of exposition, we will assume below that $N_c = 1$, and thus drop the indices β in the terms $a_\beta^{i,j,t}(\theta)$ and b_β^i , i.e.:

$$\mathcal{A}(\theta) = \bigcup_{i,j \in [N], j \neq i, t \in [T]} \{x \in \mathbb{R}^n : a_\beta^{i,j,t}(\theta)^\top x < b_\beta^i(\theta)\}. \quad (36)$$

We begin by first analyzing the hypothetical setting where the avoid set consists of a single affine-parameterized scalar constraint, i.e.,

$$\mathcal{A}(\theta) = \{x \in \mathbb{R}^n : a(\theta)^\top x < b(\theta)\}, \quad (37)$$

before restoring the unions over indices $t \in [T]$, and $i, j \in [N]$ s.t. $j \neq i$ in (36). In short, we temporarily ignore the variables $i, j \in [N]$ and $t \in [T]$. Note that, as a byproduct of the above simplification, all binary variables q introduced in (32) (for linearization purposes) can be set to 1, and hence are dropped from our notation throughout our discussion of the scalar constraint setting.

Unlike the setting of offset-parameterized avoid sets (Section B.1), the stationarity conditions formulated using the avoid set (37) will exhibit bilinearity, since they will contain terms of the form $\lambda_{d,\gamma_k} \nabla_{\xi^i} g_{\gamma_k}(\xi, \theta)$, which in turn are products of the primal variable θ and the dual variable λ (corresponding to the inequality constraints). Thus, a mixed-integer bilinear program (MIBLP) must be solved to infer θ , since products of continuous variables cannot be linearized exactly. However, we can still relax the resulting MIBLP into an MILP. Concretely, we introduce a new vector variable $\ell := (\ell_d \in \mathbb{R} : d \in [D]) \in \mathbb{R}^D$, where each ℓ_d represents the term $\lambda_{d,\gamma_k} \nabla_{\xi^i} g_{\gamma_k}(\xi, \theta)$, and a new vector variable $z_1 := (z_{d,1} \in \mathbb{R} : d \in [D]) \in \mathbb{R}^D$, which (as in the offset-parameterized case) forces λ_{d,γ_k} to be 0 when $z_{d,1} = 0$. We then replace each bilinear term of the form $\lambda_{d,\gamma_k} \nabla_{\xi^i} g_{\gamma_k}(\xi, \theta)$ with the bilinear term $\ell_d z_{d,1}$. Note that the relaxation gap introduced by the above process is non-zero only when the Lagrange multipliers λ_{d,γ_k} (and hence the binary variables $z_{d,1}$) are non-zero, i.e., when the interaction demonstration ξ_d^{loc} is active; otherwise, the bilinear term $\lambda_{d,\gamma_k} \nabla_{\xi^i} g_{\gamma_k}(\xi, \theta)$ vanishes from the stationarity conditions.

Effectively, the relaxation process introduced above replaces a product of two continuous variables, i.e., $\lambda_{d,\gamma_k} \nabla_{\xi^i} g_{\gamma_k}(\xi, \theta)$, with a product of a continuous variable and a binary variable, i.e., $\ell_d z_{d,1}$, with nonzero relaxation gap only when the associated constraints are active. We can now proceed to linearize $\ell_d z_{d,1}$ in the manner described in Section B.1. Specifically, we introduce slack variables $r := (r_d \in \mathbb{R} : d \in [D]) \in \mathbb{R}^D$ and constrain them using an appropriate analog of (32), for some positive integers $M, \underline{M}, \bar{M} > 0$. In summary, by concatenating r_d , $z_{d,1}$, and ℓ_d horizontally across indices $d \in [D]$ to form the vectors r , z_1 , and ℓ respectively, we obtain the following *relaxed* constraint inference problem for the setting of a single affine-parameterized scalar constraint:

$$\text{find } \theta, \lambda_k, \lambda_{\gamma_k}, \nu, r, z_1, z_2, \ell \quad (38a)$$

$$\text{s.t. } g_{\gamma_k}(\xi_d^{\text{loc}}, \theta) \leq 0, \quad \forall d \in [D], \quad (38b)$$

$$\lambda_k, \lambda_{\gamma_k} \geq 0, \quad (38c)$$

$$\begin{bmatrix} \lambda_{d,\gamma_k} \\ -g_{\gamma_k}(\xi_d^{\text{loc}}, \theta) \end{bmatrix} \leq M \begin{bmatrix} z_{d,1} \\ z_{d,2} \end{bmatrix}, \quad \forall d \in [D], \quad (38d)$$

$$z_{d,1} + z_{d,2} \leq 1, \quad \forall d \in [D], \quad (38e)$$

$$\nabla_{\xi^i} J^i(\xi_d^{\text{loc}}) + (\lambda_{d,k})^\top \nabla_{\xi^i} \mathbf{g}_k(\xi_d^{\text{loc}}) + r_d + \nu_d \nabla_{\xi^i} \mathbf{h}(\xi_d^{\text{loc}}) = 0, \quad \forall i \in [N], d \in [D], \quad (38f)$$

$$\min\{0, \underline{M}\} \mathbf{1} \leq r_d \leq \bar{M} \mathbf{1}, \quad \forall d \in [D], \quad (38g)$$

$$\underline{M} z_{d,1} \leq r_d \leq \bar{M} z_{d,1}, \quad \forall d \in [D], \quad (38h)$$

$$\ell_d - (\mathbf{1} - z_{d,1}) \bar{M} \leq r_d \leq \ell_d - (\mathbf{1} - z_{d,1}) \underline{M}, \quad \forall d \in [D], \quad (38i)$$

$$r_{d,1} \leq \ell_d + (\mathbf{1} - z_{d,1}), \quad \forall d \in [D], \quad (38j)$$

C. Theoretical Analysis and Proofs

In this appendix, we will first present theoretical results showing that our algorithm provides an 1) inner approximation of the true safe set and 2) outer approximation of the true unsafe set (App. C.1), which enables robust safety for downstream planning. Then, we will present theoretical results describing some of the limits of constraint learnability in the multi-agent setting (App. C.3).

1) *Theoretical Guarantees for Inner- (Outer-) Approximating Safe (Unsafe) Sets:* The following results in this subsection (i.e., Section C.1) are direct analogs of the theoretical analysis in Section V-A of [1] for the multi-agent setting, and are included for completeness. Specifically, we prove that the methods presented in (7) and (38) are guaranteed to recover inner approximations (i.e., conservative estimates) of the set of trajectories $\mathcal{S}(\theta^*)$ which obey the true, unknown constraints $\mathbf{g}_{\gamma_k}(\xi, \theta^*) \leq 0$, as well as inner approximations of the set of trajectories $\mathcal{A}(\theta^*)$ which violate $\mathbf{g}_{\gamma_k}(\xi, \theta^*) \leq 0$.

Next, we show that in the setting of affine-parameterized constraint sets, the solution to (38) likewise provides an inner approximation to the true feasible set. Below, to disambiguate between the solutions of the MINLP originally associated with the affine-parameterized constraints in Section B.2 (i.e., without the relaxation involving the new variables r , z , and

ℓ), we will denote the subset of parameters consistent with the demonstrations \mathcal{D} under the *original MINLP problem* by $\mathcal{F}_{\text{MINLP}}(\mathcal{D})$, and the subset of parameters consistent with the demonstrations \mathcal{D} under the *relaxed problem* by $\mathcal{F}_{\text{R}}(\mathcal{D})$. Similarly, we will denote the guaranteed safe set learned by solving the original MINLP problem by $\mathcal{G}_{s,\text{MINLP}}(\mathcal{D})$, and the guaranteed safe set learned by solving the relaxed problem by $\mathcal{G}_{s,\text{R}}(\mathcal{D})$.

Theorem 5: (Conservativeness of Safe and Unsafe Set Recovery from (38)) Given any set \mathcal{D} of interaction demonstrations at local Nash stationarity, the solution to (38) generates a learned guaranteed safe set $\mathcal{G}_{s,\text{R}}(\mathcal{D})$ and a learned guaranteed unsafe set $\mathcal{G}_{\neg s,\text{R}}(\mathcal{D})$ satisfying $\mathcal{G}_{s,\text{R}}(\mathcal{D}) \subseteq \mathcal{S}(\theta^*)$ and $\mathcal{G}_{\neg s,\text{R}}(\mathcal{D}) \subseteq \mathcal{A}(\theta^*)$.

Proof: Since $\mathcal{F}_{\text{MINLP}}$ denotes the set of parameters consistent with the original problem (pre-relaxation), Theorem 1 implies that $\mathcal{G}_{s,\text{MINLP}}(\mathcal{D}) \subseteq \mathcal{S}(\theta^*)$ and $\mathcal{G}_{\neg s,\text{MINLP}}(\mathcal{D}) \subseteq \mathcal{A}(\theta^*)$. Thus, it suffices to show that $\mathcal{G}_{s,\text{R}}(\mathcal{D}) \subseteq \mathcal{G}_{s,\text{MINLP}}(\mathcal{D})$ and $\mathcal{G}_{\neg s,\text{R}}(\mathcal{D}) \subseteq \mathcal{G}_{\neg s,\text{MINLP}}(\mathcal{D})$. By definition:

$$\begin{aligned}\mathcal{G}_{s,\text{R}}(\mathcal{D}) &:= \bigcap_{\theta \in \mathcal{F}_{\text{R}}(\mathcal{D})} \{\xi \in \mathbb{R}^{(n+m)T} : \mathbf{g}(\xi, \theta) > 0\} \\ \mathcal{G}_{s,\text{MINLP}}(\mathcal{D}) &:= \bigcap_{\theta \in \mathcal{F}_{\text{MINLP}}(\mathcal{D})} \{\xi \in \mathbb{R}^{(n+m)T} : \mathbf{g}(\xi, \theta) > 0\}.\end{aligned}$$

Thus, to show that $\mathcal{G}_{s,\text{R}}(\mathcal{D}) \subseteq \mathcal{G}_{s,\text{MINLP}}(\mathcal{D})$, it suffices to show that $\mathcal{F}_{\text{MINLP}}(\mathcal{D}) \subseteq \mathcal{F}_{\text{R}}(\mathcal{D})$, which in turn holds true, since relaxing the original problem enlarges the set of feasible parameters. We therefore have $\mathcal{G}_{s,\text{MINLP}}(\mathcal{D}) \subseteq \mathcal{S}(\theta^*)$, and through a similar chain of logic, $\mathcal{G}_{\neg s,\text{MINLP}}(\mathcal{D}) \subseteq \mathcal{A}(\theta^*)$. ■

2) Volume Extraction of Safe Trajectories for Motion Planning: First, we prove that the volume extraction methods formulated in Section IV-C yield inner approximations of the true, unknown inequality constraint set $\mathcal{S}(\theta^*) := \{\xi \in \mathbb{R}^{(n+m)T} : \mathbf{g}(\xi, \theta^*) \leq 0\}$.

Theorem 6: (Volume Extraction over Trajectories Generates Conservative Safe Set) Let $\mathcal{Q}_\xi := \{\xi_q : q \in [Q_\xi]\}$ denote a set of query trajectories, and let $\{\epsilon_q : q \in [Q_\xi]\}$ denote the minimum objective values obtained by solving (20) using each queried trajectory. Then (21) holds.

Proof: Suppose by contradiction that (21) is false, i.e., there exists some $q \in [Q_\xi]$ such that $\epsilon_q > 0$, and some $\xi' \in B_{\epsilon_q}^\infty(\xi_q)$ such that $\xi' \notin \mathcal{G}_s(\mathcal{D})$. By definition of $\mathcal{G}_s(\mathcal{D})$ (as given by (9)) and $\mathcal{F}(\mathcal{D})$, there exists some $\theta, \boldsymbol{\lambda}_k, \boldsymbol{\lambda}_{\neg k}$, and $\boldsymbol{\nu}$ such that $(\theta, \boldsymbol{\lambda}_k, \boldsymbol{\lambda}_{\neg k}, \boldsymbol{\nu}) \in \text{KKT}(\mathcal{D})$ but $\mathbf{g}(\xi', \theta) > 0$. Thus, $(\xi', \theta, \boldsymbol{\lambda}_k, \boldsymbol{\lambda}_{\neg k}, \boldsymbol{\nu})$ is feasible for (20), and so the solution for (20), given by ϵ_q , is less than or equal to $\|\xi' - \xi_q\|_\infty$, contradicting the fact that $\xi' \in B_{\epsilon_q}^\infty(\xi_q)$. ■

Next, we prove that the volume extraction methods formulated in Sec. IV-C yield inner approximations of the true, unknown inequality constraint set $\mathcal{S}(\theta^*) := \{\xi \in \mathbb{R}^{(n+m)T} : \mathbf{g}(\xi, \theta^*) \leq 0\}$.

Theorem 7: (Volume Extraction over Parameters Generates Conservative Safe Set) Let $\{\theta_q : q \in [Q_\theta]\}$ denote a set of queried parameters, and let $\{r_q : q \in [Q_\theta]\}$ denote the minimum objective values obtained by solving (22) using each queried trajectory. Then (23) holds.

Proof: By definition of $\mathcal{G}_s(\mathcal{D})$ in (9), it suffices to prove that:

$$\mathcal{F}(\mathcal{D}) \setminus \bigcup_{q \in [Q_\theta]} B_{r_q}^\infty(\theta_q) = \mathcal{F}(\mathcal{D}),$$

or equivalently, that:

$$\mathcal{F}(\mathcal{D}) \cap \left(\bigcup_{q \in [Q_\theta]} B_{r_q}^\infty(\theta_q) \right) = \emptyset. \quad (39)$$

Suppose by contradiction that (39), i.e., there exists some $q \in [Q_\theta]$, $\theta' \in \mathbb{R}^{(n+m)T}$ such that $r_q > 0$ and $\theta' \in B_{r_q}^\infty(\theta_q) \cap \mathcal{F}(\mathcal{D})$. By definition of $\mathcal{F}(\mathcal{D})$, there exist $\boldsymbol{\lambda}_k, \boldsymbol{\lambda}_{\neg k}, \boldsymbol{\nu}$ such that $(\theta', \boldsymbol{\lambda}_k, \boldsymbol{\lambda}_{\neg k}, \boldsymbol{\nu}) \in \text{KKT}(\mathcal{D})$, i.e., such that $(\theta', \boldsymbol{\lambda}_k, \boldsymbol{\lambda}_{\neg k}, \boldsymbol{\nu})$ lies in the feasible set of (22). Thus, the solution for (20), as given by r_q , is less than or equal to $\|\theta' - \theta_q\|_\infty$, contradicting the fact that $\theta' \in B_{r_q}^\infty(\theta_q)$. ■

The guaranteed unsafe set $\mathcal{G}_{\neg s}$ can be similarly characterized via a volume extraction procedure over the parameter space.

Above, we have established guarantees that our volume extraction method will always recover the safe set \mathcal{G}_s and the avoid set $\mathcal{G}_{\neg s}$ either accurately or conservatively, as well as conditions under which the constraint parameter θ can never be fully recovered, thus establishing theoretical limitations on learnability. Regardless, since the extracted estimates of \mathcal{G}_s and $\mathcal{G}_{\neg s}$ (termed $\hat{\mathcal{G}}_s$ and $\hat{\mathcal{G}}_{\neg s}$ below, respectively) either equal or are inner approximations of \mathcal{G}_s and $\mathcal{G}_{\neg s}$, respectively, they can be directly used by a motion planner downstream to verify constraint satisfaction or violation. Alternatively, a motion planner can design safe trajectories with *implicit* constraint checking, e.g., via Model Predictive Path Integral (MPPI) control [27]. More details are provided in App. D. In particular, any generated trajectory in $\hat{\mathcal{G}}_s$ is guaranteed to be safe, while any trajectory outside $\hat{\mathcal{G}}_{\neg s}$ is at least not guaranteed to be unsafe.

3) Theoretical Limitations of Learnability: Finally, we analyze the limitations of multi-agent constraint learning in settings in which some agents have constraints that are strictly more lax than the constraints of other agents, and are thus undetectable from interaction demonstrations at local Nash stationarity. As an example, consider interactions between two agents (Agents 1 and 2), in which Agent 1 is constrained to maintain a distance of $\theta_1 = 1$ meter away from Agent 2 at all times, while Agent 2 is constrained to maintain a distance of $\theta_2 = 2$ meters away from Agent 1 at all times. Since $\theta_2 > \theta_1$, the two agents will maintain a distance of $\theta_2 = \theta_2$ meters apart at all times in any local Nash stationary interaction. Thus, from demonstrations of local Nash stationary interactions, it would be impossible to disambiguate Agent 1's constraint parameter ($\theta_1 = 1$) from any other possible constraint parameter for Agent 1 (e.g., $\theta_1 = 1.5$) that is also consistent with all interactions at local Nash stationarity between the two agents. Therefore, θ_1 can never be precisely recovered from local Nash interactions.

We introduce the following theorem to concretely characterize this intuition. Let $\mathcal{D}(\theta)$ denote the set of all local

Nash stationary equilibrium trajectories corresponding to the constraints $\mathbf{h}(\xi) = 0$, $\mathbf{g}_k(\xi) \leq 0$, and $\mathbf{g}_{\gamma_k}(\xi, \theta) \leq 0$, i.e.,:

$$\begin{aligned} \mathcal{D}(\theta) := \{ \xi \in \mathbb{R}^{(n+m)T} : \exists \lambda_k, \lambda_{\gamma_k}, \nu \\ \text{s.t. } (\theta, \lambda_k, \lambda_{\gamma_k}, \nu) \in \text{KKT}(\{\xi\}) \}. \end{aligned} \quad (40)$$

Suppose the true, unknown constraint vector $\mathbf{g}_{\gamma_k}(\xi, \theta^*)$ can be partitioned into two components, $\mathbf{g}_{\gamma_k}^{(1)}(\xi, \theta^*)$ and $\mathbf{g}_{\gamma_k}^{(2)}(\xi, \theta^*)$, where the constraint $\mathbf{g}_{\gamma_k}^{(2)}(\xi, \theta^*) \leq 0$ is strictly looser than the remaining constraints $\mathbf{h}(\xi) = 0$, $\mathbf{g}_k(\xi) \leq 0$, $\mathbf{g}_{\gamma_k}^{(1)}(\xi, \theta^*) \leq 0$, in the sense described below:

$$\begin{aligned} \{ \xi \in \mathbb{R}^{(n+m)T} : \mathbf{h}(\xi) = 0, \mathbf{g}_k(\xi) \leq 0, \\ \mathbf{g}_{\gamma_k}^{(1)}(\xi, \theta^*) \leq 0 \} \subseteq \{ \xi \in \mathbb{R}^{(n+m)T} : \mathbf{g}_{\gamma_k}^{(2)}(\xi, \theta^*) < 0 \}. \end{aligned} \quad (41)$$

Then, for any parameter value θ satisfying:

$$\mathbf{g}_{\gamma_k}^{(1)}(\cdot, \theta^*) = \mathbf{g}_{\gamma_k}^{(1)}(\cdot, \theta), \quad (42)$$

$$\begin{aligned} \{ \xi \in \mathbb{R}^{(n+m)T} : \mathbf{h}(\xi) = 0, \mathbf{g}_k(\xi) \leq 0, \mathbf{g}_{\gamma_k}^{(1)}(\xi, \theta^*) \leq 0 \} \\ \subseteq \{ \xi \in \mathbb{R}^{(n+m)T} : \mathbf{g}_{\gamma_k}^{(2)}(\xi, \theta) < 0 \}, \end{aligned} \quad (43)$$

we will prove that $\mathcal{D}(\theta^*) = \mathcal{D}(\theta)$. In words, each local Nash stationary demonstration corresponding to the constraint parameter θ^* is also at local Nash stationarity under the constraint parameter θ , and vice versa. Thus, from the perspective of constraint learning from demonstrations, the parameter value θ will always remain as a valid alternative to the true parameter value θ^* .

Below, we repeat the statement of Thm. 4 for convenience and present its proof.

Theorem 8 (Limitations of Learnability): Let $\mathbf{g}_{\gamma_k}^{(1)}$ and $\mathbf{g}_{\gamma_k}^{(2)}$ denote a partition of the components of the unknown constraint \mathbf{g}_{γ_k} (i.e., $(\mathbf{g}_{\gamma_k}^{(1)}, \mathbf{g}_{\gamma_k}^{(2)})$ is a re-ordering of \mathbf{g}_{γ_k}) such that (25) holds, i.e.,:

$$\begin{aligned} \{ \xi \in \mathbb{R}^{(n+m)T} : \mathbf{h}(\xi) = 0, \mathbf{g}_k(\xi) \leq 0, \mathbf{g}_{\gamma_k}^{(1)}(\xi, \theta^*) \leq 0 \} \\ \subseteq \{ \xi \in \mathbb{R}^{(n+m)T} : \mathbf{g}_{\gamma_k}^{(2)}(\xi, \theta^*) < 0 \}. \end{aligned}$$

Then, for any $\theta \in \Theta$ satisfying (26) and (27), i.e.,:

$$\mathbf{g}_{\gamma_k}^{(1)}(\cdot, \theta^*) = \mathbf{g}_{\gamma_k}^{(1)}(\cdot, \theta),$$

$$\begin{aligned} \{ \xi \in \mathbb{R}^{(n+m)T} : \mathbf{h}(\xi) = 0, \mathbf{g}_k(\xi) \leq 0, \mathbf{g}_{\gamma_k}^{(1)}(\xi, \theta^*) \leq 0 \} \\ \subseteq \{ \xi \in \mathbb{R}^{(n+m)T} : \mathbf{g}_{\gamma_k}^{(2)}(\xi, \theta) < 0 \}. \end{aligned}$$

we have $\mathcal{D}(\theta^*) = \mathcal{D}(\theta)$.

Proof: Fix $\xi \in \mathcal{D}(\theta)$ arbitrarily; we aim to show that $\xi \in \mathcal{D}(\theta^*)$. Since $\xi \in \mathcal{D}(\theta)$, there exist $\lambda_k, \lambda_{\gamma_k}^{(1)}, \lambda_{\gamma_k}^{(2)}$, and ν such that $(\theta, \lambda_k, \lambda_{\gamma_k}^{(1)}, \lambda_{\gamma_k}^{(2)}) \in \text{KKT}(\{\xi\})$, i.e., for each $i \in [N]$:

$$\mathbf{h}^i(\xi) = 0, \mathbf{g}_k^i(\xi) \leq 0, \mathbf{g}_{\gamma_k}^{i,(1)}(\xi, \theta) \leq 0, \mathbf{g}_{\gamma_k}^{i,(2)}(\xi, \theta) \leq 0, \quad (44a)$$

$$\lambda_k^i, \lambda_{\gamma_k}^{i,(1)}, \lambda_{\gamma_k}^{i,(2)} \geq 0, \quad (44b)$$

$$\lambda_k^i \odot \mathbf{g}_k^i(\xi) = 0, \lambda_{\gamma_k}^i \odot \mathbf{g}_{\gamma_k}^{i,(1)}(\xi, \theta) = 0, \quad (44c)$$

$$\lambda_{\gamma_k}^{i,(2)} \odot \mathbf{g}_{\gamma_k}^{i,(2)}(\xi, \theta) = 0,$$

$$\begin{aligned} \nabla_{\xi^i} J^i(\xi) + (\lambda_k^i)^\top \nabla_{\xi^i} \mathbf{g}_k^i(\xi) + (\lambda_{\gamma_k}^{i,(1)})^\top \nabla_{\xi^i} \mathbf{g}_{\gamma_k}^{i,(1)}(\xi, \theta) \\ + (\lambda_{\gamma_k}^{i,(2)})^\top \nabla_{\xi^i} \mathbf{g}_{\gamma_k}^{i,(2)}(\xi, \theta) \end{aligned} \quad (44d)$$

$$\begin{aligned} + (\nu^i)^\top \nabla_{\xi^i} \mathbf{h}^i(\xi) = 0. \end{aligned}$$

By (44a), (26), and (27), we have $\mathbf{g}_{\gamma_k}^{(2)}(\xi, \theta) < 0$. Substituting $\mathbf{g}_{\gamma_k}^{(2)}(\xi, \theta) < 0$ into (44c) then yields $\lambda_{\gamma_k}^{(2)} = 0$, and thus, (44d) becomes:

$$\begin{aligned} \nabla_{\xi^i} J^i(\xi) + (\lambda_k^i)^\top \nabla_{\xi^i} \mathbf{g}_k^i(\xi) + (\lambda_{\gamma_k}^{i,(1)})^\top \nabla_{\xi^i} \mathbf{g}_{\gamma_k}^{i,(1)}(\xi, \theta) \\ + (\nu^i)^\top \nabla_{\xi^i} \mathbf{h}^i(\xi) = 0. \end{aligned} \quad (45)$$

We now claim that, for each $i \in [N]$:

$$\mathbf{h}^i(\xi) = 0, \mathbf{g}_k^i(\xi) \leq 0, \mathbf{g}_{\gamma_k}^{i,(1)}(\xi, \theta^*) \leq 0, \mathbf{g}_{\gamma_k}^{i,(2)}(\xi, \theta^*) \leq 0, \quad (46a)$$

$$\lambda_k^i, \lambda_{\gamma_k}^{i,(1)}, \lambda_{\gamma_k}^{i,(2)} \geq 0, \quad (46b)$$

$$\lambda_k^i \odot \mathbf{g}_k^i(\xi) = 0, \lambda_{\gamma_k}^i \odot \mathbf{g}_{\gamma_k}^{i,(1)}(\xi, \theta^*) = 0, \quad (46c)$$

$$\lambda_{\gamma_k}^{i,(2)} \odot \mathbf{g}_{\gamma_k}^{i,(2)}(\xi, \theta^*) = 0,$$

$$\begin{aligned} \nabla_{\xi^i} J^i(\xi) + (\lambda_k^i)^\top \nabla_{\xi^i} \mathbf{g}_k^i(\xi) + (\lambda_{\gamma_k}^{i,(1)})^\top \nabla_{\xi^i} \mathbf{g}_{\gamma_k}^{i,(1)}(\xi, \theta^*) \\ + (\lambda_{\gamma_k}^{i,(2)})^\top \nabla_{\xi^i} \mathbf{g}_{\gamma_k}^{i,(2)}(\xi, \theta^*) \end{aligned} \quad (46d)$$

$$\begin{aligned} + (\nu^i)^\top \nabla_{\xi^i} \mathbf{h}^i(\xi) = 0, \end{aligned}$$

Below, we prove (46a)-(46d). To prove that (46a) holds, we first note that (44a) and (26) imply that $\mathbf{h}(\xi) = 0$, $\mathbf{g}_k(\xi) \leq 0$, and $\mathbf{g}_{\gamma_k}^{(1)}(\xi, \theta^*) \leq 0$, which, in conjunction with (25), implies that $\mathbf{g}_{\gamma_k}^{(2)}(\xi, \theta^*) < 0$. Meanwhile, (46b) is identical to (44b), and thus holds. Next, to show (46c), note that (44c) implies $\lambda_k^i \odot \mathbf{g}_k^i(\xi) = 0$ for each $i \in [N]$, (44c) and (26) implies that $\lambda_k^i \odot \mathbf{g}_{\gamma_k}^{i,(1)}(\xi, \theta) = \lambda_k^i \odot \mathbf{g}_{\gamma_k}^{i,(1)}(\xi, \theta^*) = 0$, while the fact that $\lambda_{\gamma_k}^{(2)} = 0$ implies $\lambda_{\gamma_k}^{(2)} \odot \mathbf{g}_{\gamma_k}^{i,(2)}(\xi, \theta^*) = 0$. Finally, to verify (46d), we combine the fact that $\lambda_{\gamma_k}^{(2)} = 0$, (26), and (44d) to conclude that:

$$\begin{aligned} \nabla_{\xi^i} J^i(\xi) + (\lambda_k^i)^\top \nabla_{\xi^i} \mathbf{g}_k^i(\xi) + (\lambda_{\gamma_k}^{i,(1)})^\top \nabla_{\xi^i} \mathbf{g}_{\gamma_k}^{i,(1)}(\xi, \theta^*) \\ + (\lambda_{\gamma_k}^{i,(2)})^\top \nabla_{\xi^i} \mathbf{g}_{\gamma_k}^{i,(2)}(\xi, \theta^*) + (\nu^i)^\top \nabla_{\xi^i} \mathbf{h}^i(\xi) \\ = \nabla_{\xi^i} J^i(\xi) + (\lambda_k^i)^\top \nabla_{\xi^i} \mathbf{g}_k^i(\xi) + (\lambda_{\gamma_k}^{i,(1)})^\top \nabla_{\xi^i} \mathbf{g}_{\gamma_k}^{i,(1)}(\xi, \theta) \\ + (\nu^i)^\top \nabla_{\xi^i} \mathbf{h}^i(\xi) \\ = \nabla_{\xi^i} J^i(\xi) + (\lambda_k^i)^\top \nabla_{\xi^i} \mathbf{g}_k^i(\xi) + (\lambda_{\gamma_k}^{i,(1)})^\top \nabla_{\xi^i} \mathbf{g}_{\gamma_k}^{i,(1)}(\xi, \theta) \\ + (\lambda_{\gamma_k}^{i,(2)})^\top \nabla_{\xi^i} \mathbf{g}_{\gamma_k}^{i,(2)}(\xi, \theta) + (\nu^i)^\top \nabla_{\xi^i} \mathbf{h}^i(\xi) \\ = 0. \end{aligned}$$

as desired. As a result, (46) holds, i.e., $(\theta^*, \lambda_k, \lambda_{\gamma_k}^{(1)}, \lambda_{\gamma_k}^{(2)}, \nu) \in \text{KKT}(\{\xi\})$, so $\xi \in \mathcal{D}(\theta^*)$. We have thus established that $\mathcal{D}(\theta) \subseteq \mathcal{D}(\theta^*)$.

To show that $\mathcal{D}(\theta^*) \subseteq \mathcal{D}(\theta)$, it suffices to reverse the logic of the above proof to establish (44) from (46). ■

D. Robust Motion Planning via Implicit Constraint Checking

In this appendix, we first discuss how implicit constraint verification can be used within the loop of a Model Predictive

Path Integral (MPPI) controller to plan new trajectories that are robustly safe under constraint uncertainty (App. D.1). Then, we apply this method to plan a safe trajectory for a two-agent double integrator system, with results presented in App. D.2.

1) *Model Predictive Path Integral (MPPI) Control:* In this section, we elaborate on the use of our multi-agent constraint learning framework to design robust motion plans, by performing implicit constraint verification via Model Predictive Path Integral (MPPI) control.

First, we note that multiple candidate values of the constraint parameter θ may in general be consistent with the local Nash stationarity of interaction demonstrations in a given dataset \mathcal{D} . Thus, the KKT conditions (4) only pose *necessary, but not sufficient* criteria that the true value of θ must satisfy. To design robust motion plans despite this uncertainty over θ , we perform robust constraint checking to ensure that each designed, candidate trajectory is marked safe by a θ value consistent with (4). To this end, we present an *implicit* approach for constraint checking via Model Predictive Path Integral (MPPI) control [27].

Specifically, given a nominal state-control trajectory $\xi_{\text{nom}} := (x_{\text{nom}}, u_{\text{nom}})$, we enforce constraint satisfaction by iteratively applying Algorithm 1 to update the trajectory ξ_{nom} until convergence. In each iterate of Algorithm 1, we first draw M sample controls $\{u^{(s)} : s \in [M]\}$ i.i.d. from a Gaussian distribution centered on u_{nom} , which we then unroll using the dynamics f to generate the sample state-control trajectories $\{\xi^{(s)} : s \in [M]\}$. Next, for each $\xi^{(s)}$, we wish to determine whether there exists a feasible constraint parameter value θ which is consistent with the demonstrated interactions \mathcal{D} , but not with $\xi^{(s)}$. In other words, we wish to solve the feasibility problem (7), augmented with the stipulation that the sample trajectory $\xi^{(s)}$ violates the unknown primal inequality constraints $\bigwedge_{i \in [N], j \in [N_{\gamma_k}^{\text{ineq}, i}]} \{g_{j, \gamma_k}^i(\xi^{(s)}, \theta) \leq 0\}$:

$$\text{find } \theta, \lambda_k, \lambda_{\gamma_k}, \nu, \quad (47a)$$

$$\text{s.t. } (\theta, \lambda_k, \lambda_{\gamma_k}, \nu) \in \text{KKT}(\mathcal{D}), \quad (47b)$$

$$\bigvee_{i \in [N], j \in [N_{\gamma_k}^{\text{ineq}, i}]} [g_{j, \gamma_k}^i(\xi^{(s)}, \theta) > 0]. \quad (47c)$$

If (47) returns feasible, there exists some constraint parameter value $\theta^{(s)}$ consistent with the demonstrations \mathcal{D} such that $\xi^{(s)}$ violates the inequality constraints $\bigwedge_{i, j} \{g_{j, \gamma_k}^i(\xi^{(s)}, \theta^{(s)}) \leq 0\}$. In this case, we compute the total constraint violation for each agent i , denoted c_{cv}^i below, as follows:

$$c_{\text{cv}}^i(\xi^{(s)}, \theta^{(s)}) := \sum_{j \in [N_{\gamma_k}^{\text{ineq}, i}]} \max\{g_{j, \gamma_k}^i(\xi^{(s)}, \theta^{(s)}), 0\}. \quad (48)$$

Otherwise, if (47) is infeasible, we set $c_{\text{cv}}^i(\xi^{(s)}) := 0$ for each $i \in [N]$. We then update the nominal control trajectory for each agent $i \in [N]$ by taking a weighted combination of the sample control trajectories $\{u^{(s)} : s \in [M]\}$, with weights depending on the corresponding cost value $J^i(\xi^{(s)})$

and degree of constraint violation $c_{\text{cv}}(\xi^{(s)})$:

$$\tilde{u}_{\text{nom}}^i := \frac{\sum_{s \in [M]} \exp(-J^i(\xi^{(s)}) - c_{\text{cv}}(\xi^{(s)}, \theta^{(s)})) u^{(s)}}{\sum_{s \in [M]} \exp(-J^i(\xi^{(s)}) - c_{\text{cv}}(\xi^{(s)}, \theta^{(s)}))}. \quad (49)$$

Finally, we unroll the updated nominal control trajectory $\{\tilde{u}_{\text{nom}}^i : i \in [N]\}$ to generate the updated nominal state-control trajectory $\tilde{\xi}^i$.

Algorithm 1: Inverse KKT-Guided MPPI control-based Sample Trajectory Update (1 Iterate)

Data: Nominal state-control trajectory ξ_{nom} , dynamics model f , demonstrations \mathcal{D} , number of samples M

- 1 $\{\xi^{(s)} : s \in [M]\} \leftarrow N$ sample state-control trajectories generated by perturbing ξ_{nom} via a Gaussian distribution, and enforcing the dynamics f .
- 2 **for** $s \in [M]$ **do**
- 3 Solve augmented inverse KKT problem (47)
- 4 **if** (47) is feasible **then**
- 5 $\theta^{(s)} \leftarrow$ Feasible θ value from solving (47)
- 6 $c_{\text{cv}}^i(\xi^{(s)}, \theta^{(s)}) \leftarrow (48), \forall i \in [N]$.
- 7 **else**
- 8 $c_{\text{cv}}^i(\xi^{(s)}, \theta^{(s)}) \leftarrow 0$
- 9 $\{\tilde{u}_{\text{nom}}^i : i \in [N]\} \leftarrow (49)$, using $c_{\text{cv}}^i(\xi^{(s)}, \theta^{(s)})$, $J^i(\xi^{(s)})$, and $u^{(s)}$.
- 10 $\{\tilde{\xi}_{\text{nom}}^i : i \in [N]\} \leftarrow$ Unroll $\{\tilde{u}_{\text{nom}}^i : i \in [N]\}$ using dynamics f
- 11 **return** Updated nominal state-control trajectory $\tilde{\xi}_{\text{nom}}$

2) *Model Predictive Path Integral (MPPI) Simulation:*

Below, we present a simulation result illustrating that motion plans designed using our MPPI-based planner satisfy safety guarantees. Consider the setting in which $N = 2$ agents navigate in a shared 2D environment over the time horizon $T = 10$. The state of each agent $i \in [N]$ is given by $x_t^i := (p_{x,t}^i, p_{y,t}^i, v_{x,t}^i, v_{y,t}^i) \in \mathbb{R}^4$ for each $t \in [T]$, and the system state is given by $x_t := (x_t^1, \dots, x_t^N)$. Each agent follows the double integrator dynamics discretized at intervals of $\Delta t = 1$ s. Moreover, each agent $i \in [3]$ aims to optimize the following smoothness cost:

$$J^i = \sum_{t=1}^{T-1} \left[\|p_{x,t+1}^i - p_{x,t}^i\|_2^2 + \|p_{y,t+1}^i - p_{y,t}^i\|_2^2 \right] \quad (50)$$

while ensuring that their trajectory satisfies the following spherical collision avoidance constraints at each time $t \in [T]$, which are a priori unknown to the constraint learner:

$$g_{t, \gamma_k}^i(\xi, \theta^i) = -\|p_{x,t}^i - p_{x,t}^j\|_2^2 + (\theta^i)^2 \leq 0. \quad (51)$$

Above, θ^i denotes the radius of the spherical collision avoidance set for each agent $i \in [N]$. Finally, the trajectory of each agent $i \in [N]$ is constrained by a prescribed set of origin and goal positions, given by:

$$h_t^i(\xi) = \begin{bmatrix} p_0^i - \bar{p}_o^i \\ p_T^i - \bar{p}_d^i \end{bmatrix} = 0, \quad (52)$$

where $p_t^i := (p_{x,t}^i, p_{y,t}^i)$ for each $i \in [N]$ and $t \in [T]$, while $\bar{p}_o^i \in \mathbb{R}^2$ and $\bar{p}_d^i \in \mathbb{R}^2$ respectively denote the origin and destination positions for agent i , and are fixed at the following values:

$$\bar{p}_o^1 = (0, 5), \quad \bar{p}_o^2 = (10, 5), \quad (53a)$$

$$\bar{p}_d^1 = (10, 5), \quad \bar{p}_d^2 = (0, 5). \quad (53b)$$

To evaluate our MPPI-based motion planning approach, we first generate a single demonstration trajectory using the costs and constraints given in (50)-(52), with origin and destination coordinates:

$$\bar{p}_o^1 = (10, 0), \quad \bar{p}_o^2 = (0, 10), \quad (54a)$$

$$\bar{p}_d^1 = (0, 10), \quad \bar{p}_d^2 = (10, 0). \quad (54b)$$

and ground truth constraint parameters $\theta = (\theta^1, \theta^2) = (5, 5)$. To design robust trajectories, we run Algorithm 1 for 70 iterations using $M = 16$ samples, with time horizon $T = 20$ and discretization time $\Delta t = 0.1$ s. As illustrated in Figure 8, our method generates trajectories for each agent which satisfy the spherical inter-agent collision avoidance constraints (51) with radii $\theta^1 = \theta^2 = 5$. Our Gurobi solve time was 293.36 s. Note that motion planners which use implicit constraint representations, such as MPPI-based methods, are generally much less computationally efficient compared to motion planners which directly encode learned constraints via the volume extraction-based approach. We will illustrate the direct, volume extraction-based motion planning method across numerical simulations and hardware experiments in App. E.

E. Additional Experiments and Experiment Details

Below, in Sec. E.1, we provide a table of contents describing the simulation and hardware results that will be presented throughout the remainder of this section. Then, in Sec. E.2, we introduce the dynamics and dynamics transformations used in our simulation and hardware experiments. Sec. E.3 introduces details concerning the constraint parameterizations used in our work. Finally, in Sec. E.4-E.8, we present additional experiments and experiment details that were omitted from the main body of the paper due to space limitations.

1) *Table of Contents for Simulation and Experimental Results:* Table II lists the simulation and hardware results that will be presented throughout Sec. E.4-E.8. Note that we also present the following two sets of results in Sec. E.4-E.8, although they are not listed in Table II:

- A plot of Gurobi solve times for our constraint learning method vs. the number of agents involved in the constraint learning problem (in Sec. V-B and E.4.)
- Numerical results comparing our constraint learning-based method to the cost inference-based baseline [4] (in Sec. V-B and E.4).

2) *Dynamics:* In Sec. V, we presented numerical simulations involving systems with single and double integrator dynamics, unicycle dynamics, and quadcopter dynamics, as well as hardware experiments involving unicycle dynamics.

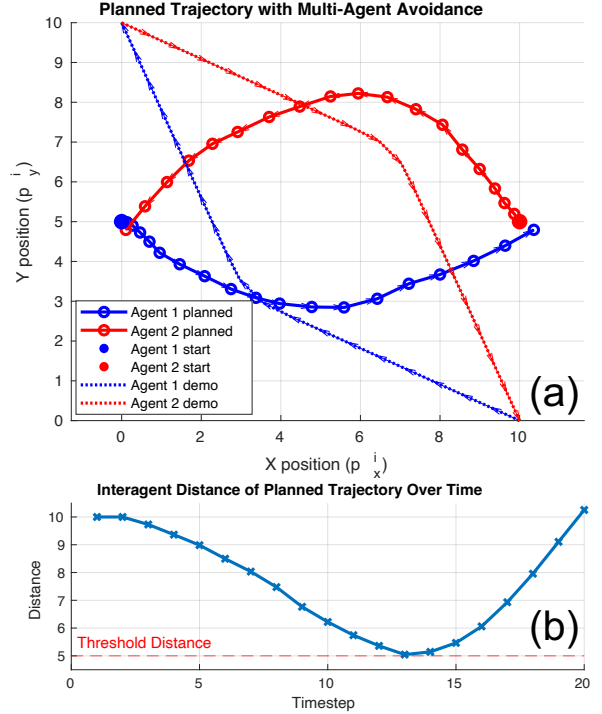


Fig. 8: (a) The multi-agent trajectories & (b) inter-agent distance checking w.r.t ground truth threshold. The planner can sample trajectories that satisfy *unknown or intangible* constraints embedded in the demonstration, without explicitly solving for the actual constraint parameters.

Below, we elaborate on implementation details pertaining to the unicycle and quadcopter dynamics. In this subsection, for ease of exposition, we omit all agent and time indices that usually accompany state and control variables in this work.

a) *Unicycle Dynamics:* We use the 4-dimensional unicycle dynamics model for ground robots, which is conventionally formulated using a state vector $x = (p_x, p_y, \phi, v) \in \mathbb{R}^4$ and a control vector $u = (u_1, u_2) \in \mathbb{R}^2$, where p_x, p_y, ϕ, v denote the x -position, y -position, heading, velocity of a 2D agent, respectively. The dynamics equations are given by:

$$\dot{p}_x = v \cos \phi, \quad (55a)$$

$$\dot{p}_y = v \sin \phi, \quad (55b)$$

$$\dot{\phi} = u_1, \quad (55c)$$

$$\dot{v} = u_2. \quad (55d)$$

To formulate the line-of-sight constraints considered in this work as affine-parameterized constraints, we introduce the variables $(v_x, v_y) \in \mathbb{R}^2$, which encode the velocity vector and relate to the state $x = (p_x, p_y, \phi, v) \in \mathbb{R}^4$ via the following polar-to-Cartesian coordinate transformation:

$$v_x := v \cos \phi,$$

$$v_y := v \sin \phi.$$

We then introduce the modified state variable $\bar{x} := (p_x, p_y, v_x, v_y) \in \mathbb{R}^4$, which evolves according to the re-

Numerical Simulations		
Dynamics	Constraint type	Sections
Double Integrator	Polytopic Collision-Avoidance	V-B, E.4
	Elliptic Collision-Avoidance	V-B, E.4
	Velocity-Dependent Spherical Collision-Avoidance	V-B, E.4
Unicycle	Spherical Proximity and Collision-Avoidance	E.5
	Line-of-Sight	E.5
Quadcopter	Spherical Collision-Avoidance	V-D, E.6
	Box-Shaped Collision-Avoidance	V-D, E.6
Single Integrator	Nonlinear	E.7
	Nonlinear, with <i>a priori</i> Unknown Cost	E.7

Hardware Experiments		
Dynamics	Constraint type	Sections
Unicycle	Spherical Proximity and Collision-Avoidance	V-G, E.8
	Line-of-Sight	V-G, E.8

TABLE II: We list the simulation and hardware experiment results presented in Sec. E.4-E.8, organized by the dynamics model used and the constraint type, and points to the subsections in the main paper and the appendix where the corresponding results are described.

formulated unicycle dynamics equations⁷:

$$\dot{p}_x = v_x, \quad (56a)$$

$$\dot{p}_y = v_y, \quad (56b)$$

$$\dot{v}_x = -\frac{v_y}{\sqrt{v_x^2 + v_y^2}}u_1 + \frac{v_x}{\sqrt{v_x^2 + v_y^2}}u_2, \quad (56c)$$

$$\dot{v}_y = \frac{v_x}{\sqrt{v_x^2 + v_y^2}}u_1 + \frac{v_y}{\sqrt{v_x^2 + v_y^2}}u_2. \quad (56d)$$

b) *Quadcopter Dynamics*: We use a 12-dimensional quadcopter dynamics model, formulated using the state vector $x \in \mathbb{R}^{12}$ and control vector $u \in \mathbb{R}^4$ shown below:

$$x = (p_x, p_y, p_z, \alpha, \beta, \gamma, \dot{p}_x, \dot{p}_y, \dot{p}_z, \dot{\alpha}, \dot{\beta}, \dot{\gamma}), \quad (57)$$

$$u = (F, \tau_\alpha, \tau_\beta, \tau_\gamma), \quad (58)$$

where p_x , p_y , and p_z respectively denote the x -, y -, and z -positions of the quadcopter, while α , β , and γ denote the Euler angles of the quadcopter. The dynamics equations are given by:

$$\ddot{p}_x = -\frac{F}{m}(\sin \alpha \sin \gamma + \cos \alpha \sin \beta \cos \gamma), \quad (59a)$$

$$\ddot{p}_y = -\frac{F}{m}(\cos \alpha \sin \gamma - \sin \alpha \sin \beta \cos \gamma), \quad (59b)$$

$$\ddot{p}_z = g - \frac{F}{m} \cos \beta \cos \gamma, \quad (59c)$$

$$\ddot{\alpha} = \frac{I_y - I_z}{I_x} \dot{\beta} \dot{\gamma}, \quad (59d)$$

$$\ddot{\beta} = \frac{I_z - I_x}{I_y} \dot{\alpha} \dot{\gamma}, \quad (59e)$$

$$\ddot{\gamma} = \frac{I_x - I_y}{I_z} \dot{\alpha} \dot{\beta}, \quad (59f)$$

which can be readily rewritten into the form $\dot{x} = f(x) + g(x, u)$ for suitably defined $f : \mathbb{R}^{12} \rightarrow \mathbb{R}^{12}$ and $g : \mathbb{R}^{12} \times \mathbb{R}^4 \rightarrow \mathbb{R}^{12}$.

3) *Constraint Parameterizations*: In this section, we elaborate upon the constraint parameterizations first presented in Sec. V-A. In particular, we explicitly formulate constraint parameterizations for elliptical, spherical, and polytope-shaped (“polytopic”) collision-avoidance constraints, spherical proximity constraints, and line-of-sight constraints. We will refer to the equations below in future subsections (i.e., Sec. E.4 to E.9) when presenting ground truth constraint parameters.

In our work, the line-of-sight constraints can be expressed using the position and velocity vectors of each agent, while

⁷When $v_x = v_y = 0$, we set $\dot{v}_x = \dot{v}_y = 0$.

all remaining constraints require only the position of each agent to be specified. As stated in Sec. V-A, given the state x_t^i of agent i at time t , for any $i \in [N]$ and $t \in [T]$, we denote by p_t^i the components of x_t^i corresponding to the position coordinates of agent i at time t .

a) *Elliptic Collision-Avoidance Constraints*: By an *elliptical collision-avoidance constraint* on agent i , we refer to a constraint that compels agent i to ensure that at each time $t \in [T]$, the relative position of any other agent j with respect to the position of agent i , i.e., $p_t^j - p_t^i$, lies outside of an ellipse of fixed shape centered at the origin. For two-dimensional agents (e.g., ground robots), we encode elliptical collision avoidance constraints for each agent i with positions $p_t^i = (p_{x,t}^i, p_{y,t}^i) \in \mathbb{R}^2$ via the following parameterization of the unknown constraint set:

$$\begin{aligned} & C_{\gamma_k}^{\text{ineq},i}(\theta) \\ &= \bigwedge_{t=1}^T \bigwedge_{j \in [N] \setminus \{i\}} \left\{ - (p_t^j - p_t^i)^\top \begin{bmatrix} \theta_2^i & 0 \\ 0 & \theta_3^i \end{bmatrix} (p_t^j - p_t^i) + \theta_1^i \leq 0 \right\}, \end{aligned} \quad (60)$$

where $\theta = (\theta_k^i : i \in [N], k \in [3]) \in \mathbb{R}^{3N}$ denotes the unknown constraint parameter, with $\theta_k^i \geq 0$ for each $i \in [N]$, $k \in [3]$.

b) *Spherical Collision Avoidance and Proximity Constraints*: By a *spherical collision-avoidance constraint* on agent i , we refer to a constraint that compels agent i to ensure that at each time $t \in [T]$, the relative position of any other agent j with respect to the position of agent i , i.e., $p_t^j - p_t^i$, lies outside of a circle of fixed radius centered at the origin. Spherical collision-avoidance constraints can be viewed as special instances of elliptic collision-avoidance constraints, in which the values $\theta_2^i = \theta_3^i$ are *a priori* known to the constraint learner. The unknown constraint set for each agent $i \in [N]$ is then given by:

$$C_{\gamma_k}^{\text{ineq},i}(\theta) = \bigwedge_{t=1}^T \bigwedge_{j \in [N] \setminus \{i\}} \left\{ - \|p_t^j - p_t^i\|_2^2 + \theta_1^i \leq 0 \right\}, \quad (61)$$

where $\theta = (\theta_1^i \geq 0 : i \in [N]) \in \mathbb{R}^N$ denotes the unknown constraint parameter, with $\theta_1^i \geq 0$ for each $i \in [N]$.

By a *spherical proximity constraint* on agent i , we refer to a constraint that compels agent i to ensure that at each time $t \in [T]$, the relative position of any other agent j with respect to the position of agent i , i.e., $p_t^j - p_t^i$, lies *inside* of a circle of fixed radius centered at the origin. When we wish to encode spherical proximity constraints in addition to spherical collision-avoidance constraints, we introduce an *upper bound* on $\|p_t^j - p_t^i\|_2^2$ in (61) encoded by a set of new constraint parameters $(\theta_5^i : i \in [N])$, with $\theta_5^i > \theta_1^i$ for all $i \in [N]$. The unknown constraint set for each agent $i \in [N]$ is then given by:

$$C_{\gamma_k}^{\text{ineq},i}(\theta) = \bigwedge_{t=1}^T \bigwedge_{j \in [N] \setminus \{i\}} \left\{ \theta_1^i \leq \|p_t^j - p_t^i\|_2^2 \leq \theta_5^i \right\}, \quad (62)$$

where $\theta = (\theta_1^i, \theta_5^i : i \in [N]) \in \mathbb{R}^{2N}$ denotes the unknown constraint parameter, with $\theta_5^i > \theta_1^i \geq 0$ for each $i \in [N]$.

c) *Polytopic Collision-Avoidance Constraints*: By a *polytope-shaped (“polytopic”) proximity constraint* on agent i , we refer to a constraint that compels agent i to ensure that at each time $t \in [T]$, the relative position of any other agent j with respect to the position of agent i , i.e., $p_t^j - p_t^i$, lies outside a polytope of fixed shape that contains the origin. Polytope-shaped collision-avoidance sets for each agent $i \in [N]$ are encoded using unions of half-spaces, via the parameterization:⁸

$$C_{\gamma_k}^{\text{ineq},i}(\theta) = \bigwedge_{t=1}^T \bigwedge_{j \in [N] \setminus \{i\}} \bigvee_{\beta=1}^{N_c} \{ a_\beta(\theta)^\top (p_t^j - p_t^i) \leq b_\beta(\theta) \}. \quad (63)$$

where, for each $\beta \in [N_c]$, the terms $a_\beta(\theta)$ and $b_\beta(\theta)$ characterize one face of the polytope. As a special case, box-shaped collision avoidance constraints can be formulated as polytopic collision avoidance constraints of the form (63), with $N_c = 4$ and $\{a_\beta(\theta) : \beta \in [4]\}$ chosen so that the resulting constraint sets have boundaries that are pairwise either parallel or orthogonal.

d) *Velocity-Dependent Spherical Collision Avoidance Constraints*: By a *velocity-dependent spherical collision-avoidance constraint* enforced on agent i to prevent collisions with agent j , we refer to a spherical collision-avoidance constraint (61) whose center is shifted from agent i ’s position towards agent j ’s position whenever agent j is moving towards agent i . More specifically, a velocity-dependent spherical collision-avoidance constraint on agent i enforces that, at each time $t \in [T]$, the vector $p_t^j - p_t^i$, with $\theta_6^i > 0$, lies outside of a sphere centered at $-\theta_6^i(v_t^j - v_t^i)$, rather than at the origin. Concretely, for agents with following the modified unicycle dynamics (56) with states $\bar{x} = (p_x, p_y, v_x, v_y) = (p, v)$, velocity-dependent collision-avoidance constraints assume the following form:

$$\begin{aligned} & C_{\gamma_k}^{\text{ineq},i} \\ &= \bigwedge_{t=1}^T \bigwedge_{j \in [N] \setminus \{i\}} \left\{ - \left\| (p_t^j - p_t^i) + \theta_6^i(v_t^j - v_t^i) \right\|_2^2 + \theta_1^i \leq 0 \right\} \\ &= \bigwedge_{t=1}^T \bigwedge_{j \in [N] \setminus \{i\}} \left\{ - (\bar{x}^j - \bar{x}^i)^\top M_{VDS}(\bar{x}^j - \bar{x}^i) + \theta_1^i \leq 0 \right\}. \end{aligned} \quad (64)$$

where:

$$M_{VDS} := \begin{bmatrix} 1 & 0 & \theta_6^i & 0 \\ 0 & 1 & 0 & \theta_6^i \\ \theta_6^i & 0 & (\theta_6^i)^2 & 0 \\ 0 & \theta_6^i & 0 & (\theta_6^i)^2 \end{bmatrix} \quad (65)$$

⁸We have either $a_\beta(\theta) \in \mathbb{R}^2$ or $a_\beta(\theta) \in \mathbb{R}^3$, depending on whether the agents under consideration are two-dimensional, e.g., ground robots, or three-dimensional, e.g., quadcopters, respectively.

Although the constraints (64) are not affine in θ_6^i , we can introduce additional variables appropriately to render them affine in the resulting, expanded set of constraint parameters. Finally, we note that if $\theta_6^i = 0$, the velocity-dependent spherical collision avoidance constraint reduces to the (velocity-independent) spherical collision-avoidance constraint originally defined in (61).

The additional term $\theta_6^i(v_t^j - v_t^i)$ compels each agent i to modulate its sensitivity to the presence of any other agent j based on agent j 's speed and direction of movement relative to that of agent i . Intuitively, if agent j begins to move towards agent i , then a velocity-dependent collision avoidance constraint with $\theta_6^i > 0$ would compel agent i to increase the minimum distance it needs to maintain from agent j . In practice, both velocity-dependent and velocity-independent spherical collision-avoidance constraints should be implemented in a multi-agent system, to ensure that each agent accounts for the movements of other agents when reasoning about collision avoidance, while also enforcing a baseline level of collision avoidance against other agents regardless of their relative velocities.

e) *Line-of-Sight Constraints*: By a *line-of-sight constraint on agent i with respect to agent j* , we refer to a constraint which compels agent i to ensure that the angle between the vectors v^i and $p^j - p^i$ is sufficiently small. Conceptually speaking, agent i must constantly travel in a direction (indicated by v^i) that is sufficiently well-aligned with the location of agent j relative to itself (as given by $p^j - p^i$). As noted in Sec. V-A, line-of-sight constraints have practical significance in the context of herding, pursuit-evasion games, and other multi-agent interaction scenarios. Below, we concretely formulate line-of-sight constraints for 2-dimensional agents (e.g., ground robots) with modified unicycle dynamics, as given in (56).

For each agent $i \in [N]$, we wish to constrain the position of any other agent j relative to agent i , i.e., $p_t^j - p_t^i \in \mathbb{R}^2$, to lie within a cone-shaped area \mathcal{C}^i whose vertex lies at the origin $(0, 0)$, and whose axis is given by $v^i = (v_x^i, v_y^i) \in \mathbb{R}^2$, the velocity vector of agent i (see Fig. 9). To characterize the two boundaries of the cone, we displace the velocity vector $v^i = (v_x^i, v_y^i)$ in the direction of $(-v_y^i, v_x^i)$, a vector perpendicular to v^i . Specifically, we define the two vectors which form the boundary of the cone, denoted $u_1^i, u_2^i \in \mathbb{R}^2$ below, as follows:

$$u_1^i(\theta) := (v_x^i, v_y^i) + \theta_7^i(-v_y^i, v_x^i), \quad (66)$$

$$u_2^i(\theta) := (v_x^i, v_y^i) - \theta_7^i(-v_y^i, v_x^i), \quad (67)$$

where the unknown parameters $\theta = (\theta_7^i : i \in [N]) \in \mathbb{R}^N$, with $\theta_7^i > 0$ for each $i \in [N]$, describe the width of the cone \mathcal{C}^i , for each $i \in [N]$. Next, to constrain each relative distance vector $p_t^j - p_t^i$ to lie within \mathcal{C}^i , we will define halfspaces $H_1(\theta)$ and $H_2(\theta)$ whose boundaries are given by $u_1^i(\theta)$ and $u_2^i(\theta)$, respectively. Let $w_1^i(\theta) \in \mathbb{R}^2$ and $w_2^i(\theta) \in \mathbb{R}^2$ be vectors perpendicular to $u_1^i(\theta)$ and $u_2^i(\theta)$, respectively which point “inward” into the cone \mathcal{C}^i , as given below:

$$w_1^i(\theta) = \theta_7^i(v_x^i, v_y^i) - (-v_y^i, v_x^i), \quad (68)$$

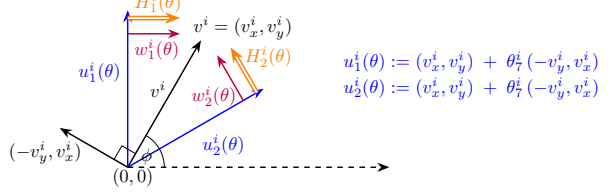


Fig. 9: Schematic for explaining the formulation of the line-of-sight constraints. In particular, we begin by defining $u_1(\theta)$ and $u_2(\theta)$ as vectors that are displaced from v^i , the velocity vector of agent i , in the orthogonal direction given by $(-v_y^i, v_x^i)$. Here, θ captures the degree to which $u_1(\theta)$ and $u_2(\theta)$ differ from v^i . Then, we define $w_1^i(\theta)$ and $w_2^i(\theta)$ to be vectors orthogonal to $u_1^i(\theta)$ and $u_2^i(\theta)$, respectively, that both point “into” the cone bounded by $u_1^i(\theta)$ and $u_2^i(\theta)$. Finally, we define $H_1^i(\theta)$ and $H_2^i(\theta)$ as the half-spaces with boundaries given by $u_1^i(\theta)$ and $u_2^i(\theta)$, by using $w_1^i(\theta)$ and $w_2^i(\theta)$ as the normal vectors of $H_1^i(\theta)$ and $H_2^i(\theta)$, respectively. Then, our desired cone \mathcal{C}^i can be given as the intersection of $H_1^i(\theta)$ and $H_2^i(\theta)$, i.e., $\mathcal{C}^i(\theta) = H_1^i(\theta) \cap H_2^i(\theta)$.

$$w_2^i(\theta) = \theta_7^i(v_x^i, v_y^i) + (-v_y^i, v_x^i). \quad (69)$$

Then the constraint set corresponding to agent i 's line-of-sight constraint can be written as:

$$\begin{aligned} & \bigwedge_{t=1} \bigwedge_{j \in [N] \setminus \{i\}} \left\{ p_t^j - p_t^i \in H_1(\theta) \cap H_2(\theta) \right\} \quad (70) \\ &= \bigwedge_{t=1} \bigwedge_{j \in [N] \setminus \{i\}} \left\{ (p_t^j - p_t^i)^\top (v_y + v_x \theta_7^i, -v_x + v_y \theta_7^i) \geq 0, \right. \\ & \quad \left. (p_t^j - p_t^i)^\top (-v_y + v_x \theta_7^i, v_x + v_y \theta_7^i) \geq 0 \right\} \\ &= \bigwedge_{t=1} \bigwedge_{j \in [N] \setminus \{i\}} \left\{ \begin{aligned} & (p_{x,t}^j - p_{x,t}^i) v_{y,t}^i - (p_{y,t}^j - p_{y,t}^i) v_{x,t}^i \\ & + [(p_{x,t}^j - p_{x,t}^i) v_{x,t}^i + (p_{y,t}^j - p_{y,t}^i) v_{y,t}^i] \theta_7^i \geq 0, \\ & - (p_{x,t}^j - p_{x,t}^i) v_{y,t}^i + (p_{y,t}^j - p_{y,t}^i) v_{x,t}^i \\ & + [(p_{x,t}^j - p_{x,t}^i) v_{x,t}^i + (p_{y,t}^j - p_{y,t}^i) v_{y,t}^i] \theta_7^i \geq 0. \end{aligned} \right\}. \end{aligned}$$

Note that the constraints formulated above in (70) are affine in the parameter θ , despite exhibiting nonlinearities (more precisely, bilinearities), in the primal variables describing positions and velocities.

f) *Origin and Goal Constraints*: As stated in Sec. V-A, each agent is prescribed a given, *known* set of origin and goal position constraints, given by:

$$\bigwedge_{i \in [N]} \{p_0^i = \bar{p}_o^i, p_T^i = \bar{p}_d^i\}, \quad (71)$$

where \bar{p}_o^i and \bar{p}_d^i denote the pre-determined origin and goal positions, respectively.

For experiments which involve line-of-sight constraints or velocity-based collision-avoidance constraints, we may wish to constrain the agents' initial and final velocities in addition

to their start and goal positions, in which case (71) becomes:

$$\bigwedge_{i \in [N]} \{p_0^i = \bar{p}_o^i, v_0^i = \bar{v}_o^i, p_T^i = \bar{p}_d^i, v_T^i = \bar{v}_d^i\}. \quad (72)$$

4) *Double Integrator Simulations*: As described in Sec. V-B, we evaluate our method on simulated interactions between agents with double integrator dynamics and either elliptic or polytopic collision-avoidance constraints, as described by (60) and (63). We also report the Gurobi solve times, for learning spherical collision-avoidance constraints, as a function of the number of interacting agents. Below, we provide the ground truth parameters and other details of the aforementioned experiments that were omitted in the main text.

a) *Elliptic Constraints*: We generate an interaction demonstration from which we learn the elliptic collision-avoidance constraint sets of two agents with double integrator dynamics (Fig. 2a). Specifically, we discretize the continuous-time double integrator dynamics at intervals of $\Delta t = 1$, and set the time horizon to be $T = 10$. We define the cost of each agent to encode the smoothness objective formulated in Sec. V-A, i.e.,

$$J^i = \sum_{t=1}^{T-1} \|p_{t+1}^i - p_t^i\|_2^2, \quad \forall i \in \{1, 2\}. \quad (73)$$

Elliptical collision-avoidance constraints of the form (60) with the following ground truth parameters, which are *a priori* unknown to the constraint learner, are enforced on each agent's trajectory:

$$(\theta_1^i, \theta_2^i, \theta_3^i) = (49, 4, 1), \quad \forall i \in \{1, 2\}.$$

The start and goal positions of each agent $i \in [2]$ are constrained via known equality constraints of the form (71) to be at \bar{p}_o^i and \bar{p}_d^i , respectively, as given below:

$$\begin{aligned} \bar{p}_o^1 &= (0.0, 0.0), & \bar{p}_d^1 &= (10.0, 10.0), \\ \bar{p}_o^2 &= (10.0, 10.0), & \bar{p}_d^2 &= (0.0, 0.0). \end{aligned}$$

We successfully recovered the *a priori* unknown constraint parameters with a Gurobi solve time of 0.2 seconds.

b) *Polytopic Collision-Avoidance Constraints*: We generate two interaction demonstrations from which we learn the polytopic collision-avoidance constraint sets of two agents with double integrator dynamics (Fig. 2b, 2c). The two demonstrations share all of the following parameter settings *except* agents' initial and final goal positions. Specifically, we discretize the continuous-time double integrator dynamics at intervals of $\Delta t = 1$, and set the time horizon to be $T = 20$. We define the cost of each agent to encode the smoothness objective formulated in Sec. V-A, i.e.,

$$J^i = \sum_{t=1}^{T-1} \|p_{t+1}^i - p_t^i\|_2^2, \quad \forall i \in \{1, 2\}.$$

Polytopic collision-avoidance constraints of the form (63) with the ground truth parameters $\{a_\beta(\theta) \in \mathbb{R}^2, b_\beta(\theta) \in \mathbb{R} : \beta \in [4]\}$ defined below, which are *a priori* unknown to the

constraint learner, are enforced on each agent's trajectory. For each $\beta \in [4]$, we set $a_\beta(\theta) \in \mathbb{R}^2$ to be the transpose of the β -th row of the matrix $A(\theta)$ defined below, and we set $b_\beta(\theta) \in \mathbb{R}$ to be the β -th entry of the vector $b(\theta)$ defined below:

$$A(\theta) = \begin{bmatrix} -0.2545 & -0.9671 \\ 0.9487 & -0.3162 \\ 0.2169 & 0.9762 \\ -0.9285 & 0.3714 \end{bmatrix}, \quad b(\theta) = \begin{bmatrix} 10.0779 \\ 9.4868 \\ 11.6058 \\ 9.4705 \end{bmatrix}.$$

The start and goal positions of each agent $i \in [2]$ are constrained via known equality constraints of the form (71) to be at \bar{p}_o^i and \bar{p}_d^i , respectively, as given below:

$$\begin{aligned} \text{Demonstration 1: } \bar{p}_o^1 &= (-2.0, 0.0), & \bar{p}_d^1 &= (9.5, 9.5), \\ & \bar{p}_o^2 &= (9.5, 9.5), & \bar{p}_d^2 &= (-2, 9.5), \\ \text{Demonstration 2: } \bar{p}_o^1 &= (15.0, 0.0), & \bar{p}_d^1 &= (15.0, 15.0), \\ & \bar{p}_o^2 &= (15.0, 15.0), & \bar{p}_d^2 &= (15.0, 0.0). \end{aligned}$$

We successfully recovered the *a priori* unknown constraint parameters with a Gurobi solve time of 54.86 seconds. The learned constraints were then used to generate safe motion plans in simulation, in conjunction with the agent costs, dynamics, time discretization, and time horizon given above, as well as equality constraints of the form (71) to enforce the following start positions \bar{p}_o^i and goal positions \bar{p}_d^i for each agent i :

$$\begin{aligned} \bar{p}_o^1 &= (15.0, 0.0), & \bar{p}_d^1 &= (0.0, 15.0), \\ \bar{p}_o^2 &= (15.0, 15.0), & \bar{p}_d^2 &= (0.0, 0.0). \end{aligned}$$

The generated safe motion plans are plotted in Fig. 2c.

c) *Velocity-Dependent Spherical Collision Avoidance Constraints*: We generate an interaction demonstration from which we learn the *velocity-dependent* spherical collision-avoidance constraint sets, of the form (64), of two agents with double integrator dynamics (Fig. 2e, 2f, and 2g). Specifically, we discretize the continuous-time double integrator dynamics at intervals of $\Delta t = 0.5$, and set the time horizon to be $T = 20$. We define the cost of each agent as follows:

$$J^i = \sum_{t=1}^T \sum_{j=1}^2 \left(\|p_{t+1}^j - p_t^j\|_2^2 + \|u_t^j\|_2^2 \right).$$

Velocity-dependent spherical collision-avoidance constraints of the form (64), with the following *a priori* unknown ground truth parameters, are enforced on the agents' trajectories:

$$\theta_1^i = 2.0, \quad \theta_6^i = 1.0, \quad \forall i \in \{1, 2\}.$$

The start position, initial velocity, goal position, and final velocity of each agent $i \in [3]$ are constrained via known equality constraints of the form (72) to be at \bar{p}_o^i , v_0^i , \bar{p}_d^i , and \bar{v}_d^i , respectively, as given below:

$$\begin{aligned} \bar{p}_o^1 &= (-3.0, 0.0), & \bar{v}_o^1 &= (0.715, 0.145), \\ \bar{p}_d^1 &= (3.0, 3.0), & \bar{v}_d^1 &= (0.546, 0.483), \\ \bar{p}_o^2 &= (3.0, 3.0), & \bar{v}_o^2 &= (-0.715, -0.145), \\ \bar{p}_d^2 &= (-3.0, 0.0), & \bar{v}_d^2 &= (-0.546, -0.483). \end{aligned}$$

We successfully recovered the *a priori* unknown constraint parameters with a Gurobi solve time of 0.12 seconds. The learned constraints were then used to generate two safe motion plans in simulation, in conjunction with the agent costs, dynamics, time discretization, and time horizon given above, but different start positions \bar{p}_o^i , initial velocities \bar{v}_o^i , goal positions \bar{p}_d^i , and final velocities \bar{v}_d^i for each agent i , as enforced by equality constraints of the form (72). In particular, for the first motion plan, as plotted in Fig. 4f, we set:

$$\begin{aligned}\bar{p}_o^1 &= (2.0, 0.0), & \bar{v}_o^1 &= (-0.622, 0.179), \\ \bar{p}_d^1 &= (-3.0, 3.0), & \bar{v}_d^1 &= (-0.439, 0.439), \\ \bar{p}_o^2 &= (-3.0, 3.0), & \bar{v}_o^2 &= (0.727, -0.179), \\ \bar{p}_d^2 &= (3.0, 0.0), & \bar{v}_d^2 &= (0.544, -0.439).\end{aligned}$$

For the second motion plan, as plotted in Fig. 4g, we set:

$$\begin{aligned}\bar{p}_o^1 &= (2.0, 0.0), & \bar{v}_o^1 &= (-0.526, 0.316), \\ \bar{p}_d^1 &= (-3.0, 3.0), & \bar{v}_d^1 &= (-0.526, 0.316), \\ \bar{p}_o^2 &= (2.0, 3.0), & \bar{v}_o^2 &= (-0.526, 0.316), \\ \bar{p}_d^2 &= (-3.0, 6.0), & \bar{v}_d^2 &= (-0.526, 0.316).\end{aligned}$$

d) Robustness of the Volume Extraction Approach Relative to Inferred Uncertainty: Below, we present an experiment which illustrates that, in terms of robustly guaranteeing safety despite incomplete recovery of the true constraints, volume extraction-informed motion plans outperform motion plans designed using a single point estimate of constraint parameter. Specifically, Fig. 10 illustrates a 2-agent interaction demonstration (blue) which activates all but the bottom edge of a box-shaped constraint. We generated (1) motion plans naively generated using an incorrect, single point estimate of the position of the bottom edge of the constraint (black), as well as (2) motion plans generated by leveraging conservative estimates of the bottom edge using volume extraction (coincides with the blue interaction demonstration). Whereas our volume-extraction based approach informed the successful design of interactive trajectories that obeyed all underlying, true constraints, the naive motion plan, generated using the incorrect point estimate of the location of the box constraint's bottom edge, violated the box constraint.

e) Gurobi Solve Times vs. Number of Interacting Agents: To illustrate the computational tractability of our constraint learning method, we record Gurobi solve times for multi-agent constraint learning problems involving different numbers of interacting agents, namely $N = 2, 4, 10, 20, 30$ (Fig. 11). In each simulation, we assume all agents have double integrator dynamics discretized at intervals of $\Delta t = 1$, and we set the time horizon to be $T = 20$. We define the cost of each agent to encode the smoothness objective formulated in Sec. V-A, i.e.,

$$J^i = \sum_{t=1}^{T-1} \|p_{t+1}^i - p_t^i\|_2^2, \quad \forall i \in \{1, 2\}.$$

Moreover, when inferring *box* collision avoidance constraints from agent demonstrations, the 2-, 4-, and 10-agent problem

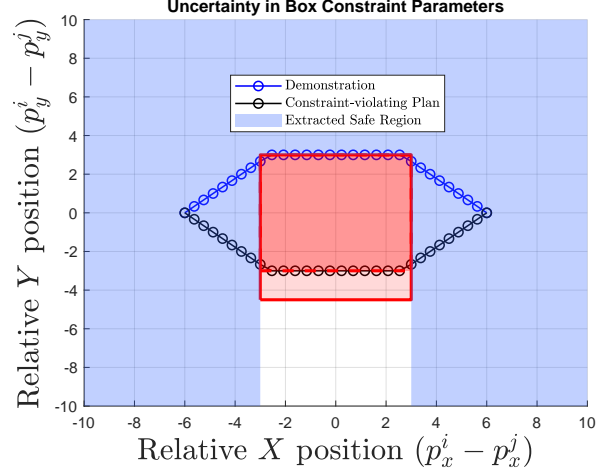


Fig. 10: An example in which a single demonstration (blue, with circles) allows the recovery of the left, top, and right edges of the true, unknown 2D box collision-avoidance constraint set (shaded dark and light red, bordered by solid red lines), but not its bottom edge, $y = -4.5$. Using volume extraction, we compute the guaranteed safe region (shaded blue), which is then used to design guaranteed safe motion plans which, in this instance, coincide with the blue demonstration. However, a naive point estimate of the constraint's bottom edge returns $y = -3$, which underestimates the extent to which the collision avoidance set extends downwards. This results in an under-approximation (shaded dark red) of the true collision avoidance set. The motion plan generated as a result (black) is constraint-violating.

instances required Gurobi solve times of 0.06 s, 0.59 s, and 5.37 s, respectively.

Spherical collision-avoidance constraints of the form (61) with the following ground truth parameters are enforced on the trajectories of all agents:

$$\theta_1^i = i, \quad \forall i \in [N] \quad (74)$$

The start and goal positions $\{p_o^i, \bar{p}_d^i : i \in [N]\}$ of the interacting agents are identically and independently drawn from a circle of radius 200 centered at the origin, and subsequently encoded into known equality constraints of the form (71).

5) Unicycle Simulations: We also evaluate our method on simulated interactions between agents with unicycle dynamics and either spherical collision-avoidance and proximity constraints, as described by (62), or line-of-sight constraints, as described by (70).

a) Spherical Proximity and Collision-Avoidance Constraints: We generate an interaction demonstration from which we learn the spherical proximity and collision-avoidance constraint sets, as given by (62), of two agents with double integrator dynamics (Fig. 4a, 4b). Specifically, we discretize the continuous-time double integrator dynamics at intervals of $\Delta t = 0.5$, and set the time horizon to be

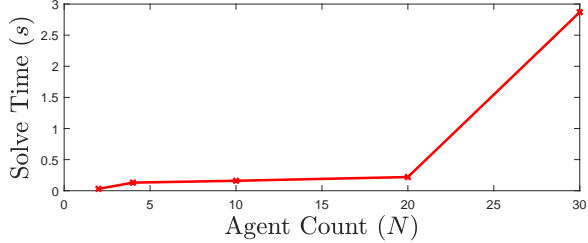


Fig. 11: Gurobi solve times for our constraint learning method, when applied to simulations involving $N = 2, 4, 10, 20, 30$ agents with double integrator dynamics and spherical collision-avoidance constraint sets. When $N \leq 20$, our method easily recovers the constraints of all agents in less than 0.25 s. When $N = 30$, our method can still recover the constraints of all agents in roughly 3s.

$T = 10$. We define the cost of each agent as follows:

$$J^i = \sum_{t=1}^T \sum_{j=1}^2 \left(\|p_{t+1}^j - p_t^j\|_2^2 + \|u_t^j\|_2^2 \right) + 5 \cdot \sum_{t=1}^T p_{y,t}^2.$$

Spherical proximity and collision-avoidance constraints of the form (62), with the following *a priori unknown* ground truth parameters, are enforced on each agent's trajectory:

$$(\theta_1^i, \theta_5^i) = (1.0, 4.0), \quad \forall i \in \{1, 2\}.$$

The start position, initial velocity, goal position, and final velocity of each agent $i \in [N]$ are constrained via known equality constraints of the form (72) to be at \bar{p}_o^i , \bar{v}_o^i , \bar{p}_d^i , and \bar{v}_d^i respectively, as given below:

$$\begin{aligned} \bar{p}_o^1 &= (-3.0, 0.0), & \bar{v}_o^1 &= (0.0, 0.1), \\ \bar{p}_d^1 &= (3.0, 3.0), & \bar{v}_o^1 &= (0.0, 0.1), \\ \bar{p}_o^2 &= (-1.95, -0.05), & \bar{v}_o^2 &= (2.35, 0.1), \\ \bar{p}_d^2 &= (2.95, 1.0), & \bar{v}_o^2 &= (0.77, 1.77). \end{aligned}$$

We successfully recovered the *a priori* unknown constraint parameters with a Gurobi solve time of 0.02 seconds. The learned constraints were then used to generate safe motion plans in simulation, in conjunction with the agent costs, dynamics, time discretization, and time horizon given above, as well as equality constraints of the form (71) to enforce the following start positions \bar{p}_o^i and goal positions \bar{p}_d^i for each agent i :

$$\begin{aligned} \bar{p}_o^1 &= (-3.0, 0.0), & \bar{v}_o^1 &= (0.0, 0.1), \\ \bar{p}_d^1 &= (1.0, 2.0), & \bar{v}_d^1 &= (2.356, 0.1), \\ \bar{p}_o^2 &= (-1.95, -0.55), & \bar{v}_o^2 &= (2.356, 0.1), \\ \bar{p}_d^2 &= (1.129, 0.004), & \bar{v}_d^2 &= (0.685, 1.349). \end{aligned}$$

The generated safe motion plans are plotted in Fig. 4b.

b) *Line-of-Sight Constraints*: We generate an interaction demonstration from which we learn the line-of-sight constraints of two agents with unicycle dynamics (Fig. 4c, 4d). Specifically, we discretize the (modified) continuous-time unicycle dynamics (56) at intervals of $\Delta t = 0.3$, and

set the time horizon to be $T = 20$. We define the cost of each agent to be as follows:

$$J^i = \sum_{t=1}^T \sum_{j=1}^2 \left(\|p_{t+1}^j - p_t^j\|_2^2 + \|u_t^j\|_2^2 \right).$$

The following constraints, which are *a priori* unknown to the constraint learner, are enforced on each agent's trajectory—Spherical proximity constraints of the form (62), with ground truth parameters:

$$(\theta_1^i, \theta_5^i) = (1.0, 16.0), \quad \forall i \in \{1, 2\},$$

and line-of-sight constraints of the form (70), with ground truth parameters:

$$\theta_7^i = 0.1, \quad \forall i \in \{1, 2\},$$

The start position, initial velocity, goal position, and final velocity of each agent $i \in [N]$ are constrained via known equality constraints of the form (72) to be at \bar{p}_o^i , \bar{v}_o^i , \bar{p}_d^i , and \bar{v}_d^i , respectively, as given below:

$$\begin{aligned} \bar{p}_o^1 &= (-3.0, 0.0), & \bar{v}_o^1 &= (0.270, 0.0), \\ \bar{p}_d^1 &= (3.0, 3.0), & \bar{v}_d^1 &= (0.855, 0.0), \\ \bar{p}_o^2 &= (-4.1, 0.0), & \bar{v}_o^2 &= (0.438, 0.0), \\ \bar{p}_d^2 &= (1.413, 2.245), & \bar{v}_d^2 &= (1.056, 0.576). \end{aligned}$$

The Gurobi solve time was 0.09 seconds. The learned constraints were then used to generate safe motion plans in simulation, in conjunction with the agent costs, dynamics, time discretization, and time horizon given above, as well as equality constraints of the form (71) to enforce the following start positions \bar{p}_o^i and goal positions \bar{p}_d^i for each agent i :

$$\begin{aligned} \bar{p}_o^1 &= (0.0, 3.0), & \bar{v}_o^1 &= (0.293, 0.0), \\ \bar{p}_d^1 &= (2.001, 0.013), & \bar{v}_d^1 &= (0.007, -0.565), \\ \bar{p}_o^2 &= (-1.2, 3.0), & \bar{v}_o^2 &= (0.210, 0.0) \\ \bar{p}_d^2 &= (0.985, 1.735), & \bar{v}_d^2 &= (-0.492, 0.238). \end{aligned}$$

The generated safe motion plans are plotted in Fig. 4d.

6) *Quadcopter Simulations*: As described in Sec. V-D, we evaluate our method on simulated interactions between agents with 12-D quadcopter dynamics and either elliptic or polytopic (in particular, box-shaped) collision-avoidance constraints, as described by (60) and (63). We also report the Gurobi solve times, for learning spherical collision-avoidance constraints, as a function of the number of interacting agents. Below, we provide the ground truth parameters and other details of the aforementioned experiments that were omitted in the main text.

a) *Spherical Collision-Avoidance Constraints*: We generate an interaction demonstration from which we learn the spherical collision-avoidance constraint sets of three agents with quadcopter dynamics (Fig. 5a and 5b). Specifically, we discretize the continuous-time quadcopter dynamics (59) at intervals of $\Delta t = 1$, and set the time horizon to be $T = 20$.

We define the cost of each agent to encode the smoothness objective formulated in Sec. V-A, i.e.,

$$J^i = \sum_{t=1}^{T-1} \|p_{t+1}^i - p_t^i\|_2^2, \quad \forall i \in \{1, 2\}.$$

Spherical collision-avoidance constraints of the form (61), with the following *a priori* unknown ground truth parameters, are enforced on the agents' trajectories:

$$\theta_1^1 = 6, \quad \theta_1^2 = 8, \quad \theta_1^3 = 9.$$

The start and goal positions of each agent $i \in [3]$ are constrained via known equality constraints of the form (71) to be at \bar{p}_o^i and \bar{p}_d^i , respectively, as given below:

$$\begin{aligned} \bar{p}_o^1 &= (0.0, 0.0, 0.0), & \bar{p}_d^1 &= (20.0, 20.0, 20.0), \\ \bar{p}_o^2 &= (20.0, 20.0, 20.0), & \bar{p}_d^2 &= (0.0, 0.0, 0.0), \\ \bar{p}_o^3 &= (0.0, 20.0, 0.0), & \bar{p}_d^3 &= (20.0, 0.0, 20.0). \end{aligned}$$

We successfully recovered the *a priori* unknown constraint parameters with a Gurobi solve time of 0.2 seconds. The learned constraints were then used to generate safe motion plans in simulation, in conjunction with the agent costs, dynamics, time discretization, and time horizon given above, as well as equality constraints of the form (71) to enforce the following start positions \bar{p}_o^i and goal positions \bar{p}_d^i for each agent i :

$$\begin{aligned} \bar{p}_o^1 &= (0.0, 0.0, 0.0), & \bar{p}_d^1 &= (10.0, 10.0, 20.0), \\ \bar{p}_o^2 &= (10.0, 10.0, 10.0), & \bar{p}_d^2 &= (0.0, 0.0, 0.0), \\ \bar{p}_o^3 &= (0.0, 10.0, 0.0), & \bar{p}_d^3 &= (20.0, 0.0, 20.0). \end{aligned}$$

The generated safe motion plans are plotted in Fig. 5b.

b) Box-Shaped Collision-Avoidance Constraints: We generate an interaction demonstration from which we learn the polytopic collision-avoidance constraint sets of four agents with quadcopter dynamics (Fig. 14b, 14c). Specifically, we discretize the continuous-time quadcopter dynamics at intervals of $\Delta t = 1$, and set the time horizon to be $T = 10$. We define the cost of each agent to encode the smoothness objective formulated in Sec. V-A, i.e.,

$$J^i = \sum_{t=1}^{T-1} \|p_{t+1}^i - p_t^i\|_2^2, \quad \forall i \in \{1, 2\}.$$

Polytopic collision-avoidance constraints of the form (63) with the *a priori* unknown ground truth parameters $\{a_\beta(\theta) \in \mathbb{R}^2, b_\beta(\theta) \in \mathbb{R} : \beta \in [4]\}$ defined below, are enforced on each agent's trajectory. For each $\beta \in [6]$, we set $a_\beta(\theta) \in \mathbb{R}^2$ to be the transpose of the β -th row of the matrix $A(\theta)$ defined below, and we set $b_\beta(\theta) \in \mathbb{R}$ to be the β -th entry of the vector $b(\theta)$ defined below:

$$A(\theta) = \begin{bmatrix} 1.0 & 0.0 & 0.0 \\ -1.0 & 0.0 & 0.0 \\ 0.0 & 1.0 & 0.0 \\ 0.0 & -1.0 & 0.0 \\ 0.0 & 0.0 & 1.0 \\ 0.0 & 0.0 & -1.0 \end{bmatrix}, \quad b(\theta) = \begin{bmatrix} -6.0 \\ -6.0 \\ -6.0 \\ -6.0 \\ -4.0 \\ -4.0 \end{bmatrix}.$$

The start and goal positions of each agent $i \in [2]$ are constrained via known equality constraints of the form (71) to be at \bar{p}_o^i and \bar{p}_d^i , respectively, as given below:

$$\begin{aligned} \bar{p}_o^1 &= (0.0, 0.0, 0.0), & \bar{p}_d^1 &= (10.0, 10.0, 10.0), \\ \bar{p}_o^2 &= (10.0, 10.0, 10.0), & \bar{p}_d^2 &= (0.0, 0.0, 0.0), \\ \bar{p}_o^3 &= (0.0, 10.0, 0.0), & \bar{p}_d^3 &= (10.0, 0.0, 10.0), \\ \bar{p}_o^4 &= (10.0, 0.0, 10.0), & \bar{p}_d^4 &= (0.0, 10.0, 0.0). \end{aligned}$$

We successfully recovered the *a priori* unknown constraint parameters with a Gurobi solve time of 1.67 seconds. The learned constraints were then used to generate safe motion plans in simulation, in conjunction with the agent costs, dynamics, time discretization, and time horizon given above, as well as equality constraints of the form (71) to enforce the following start positions \bar{p}_o^i and goal positions \bar{p}_d^i for each agent i :

$$\begin{aligned} \bar{p}_o^1 &= (7.0, -7.0, -7.0), & \bar{p}_d^1 &= (-7.0, 7.0, 7.0), \\ \bar{p}_o^2 &= (0.0, 7.0, 7.0), & \bar{p}_d^2 &= (7.0, -7.0, -7.0). \end{aligned}$$

The generated safe motion plans are plotted in Fig. 14c.

c) Comparison Against the Single-Agent Constraint Learning Approach in [1]: As shown in the 3-quadcopter interaction demonstrations illustrated in Fig. 5 (Sec. V), our game-theoretic approach correctly deduces that Agent 2's constraint avoidance radius is 8, and that the larger gap of 9 between the trajectories of Agents 2 and 3 should be attributed to Agent 3 instead. As a baseline comparison, a single-agent constraint inference method applied to the same problem failed to accurately recover the constraint radius of Agent 2 with zero stationarity error (specifically, with stationarity error equal to 1.8). The reason for this failure is that the single-agent constraint learning method for recovering Agent 2's constraints treats the other two agents as moving obstacles without intents and constraints of their own. As a result, assigning Agent 2 a constraint radius of 9 would lead to the conclusion that Agent 2 behaved suboptimally in Agent 1's vicinity, while assigning Agent 2 a constraint radius of 8 would lead to the conclusion that Agent 2 violated their constraint in Agent 3's vicinity.

Remark 4: Alternatively, one can consider a single-agent inverse optimal control framework, in which one sums across all agent costs to define a system-level cost $J(\xi) := \sum_{i=1}^N J^i(\xi)$, and applies the single-agent constraint inference method presented in [1] to attempt to learn all agents' constraints at once. Concretely, consider the following feasibility problem of searching for valid parameter values θ that are consistent with the following KKT conditions, across all agent indices $i \in [N]$. The following equations can essentially be regarded as a centralized, single-agent version of the KKT conditions for our multi-agent constraints, as presented in (4):

$$\mathbf{h}^i(\xi) = 0, \quad \mathbf{g}_k^i(\xi) \leq 0, \quad \mathbf{g}_{\gamma_k}^i(\xi, \theta) \leq 0, \quad (75a)$$

$$\boldsymbol{\lambda}_{d,k}^i, \boldsymbol{\lambda}_{d,\gamma_k}^i \geq 0, \quad (75b)$$

$$\boldsymbol{\lambda}_{d,k}^i \odot \mathbf{g}_k^i(\xi) = 0, \quad \boldsymbol{\lambda}_{d,\gamma_k}^i \odot \mathbf{g}_{\gamma_k}^i(\xi, \theta) = 0, \quad (75c)$$

$$\nabla_{\xi} J(\xi) + (\boldsymbol{\lambda}_{d,k}^i)^\top \nabla_{\xi} \mathbf{g}_k^i(\xi) + (\boldsymbol{\lambda}_{d,\gamma_k}^i)^\top \nabla_{\xi} \mathbf{g}_{\gamma_k}^i(\xi, \theta) + (\boldsymbol{\nu}_d^i)^\top \nabla_{\xi} \mathbf{h}^i(\xi) = 0. \quad (75d)$$

However, we empirically verified that for a 2-agent interaction setting, the inverse optimization problem characterized by (75) produced a stationarity error value of 2.5, thus likewise incorrectly concluding that the supplied demonstrations were not at Nash stationarity. These results were obtained using single-integrator dynamics, with $T = 7$, and with the following start and goal positions for each agent:

$$\begin{aligned} \bar{p}_o^1 &= (0.0, 3.0), & \bar{p}_d^1 &= (0.0, -3.0), \\ \bar{p}_o^2 &= (0.0, -3.0), & \bar{p}_d^2 &= (0.0, 3.0). \end{aligned}$$

Agent 1's constraint was defined to ensure that $\|x_t^1 - x_t^2\|_2 \geq 1$ for all $t \in [T]$, while Agent 2's constraint was defined to ensure that $\|x_t^1 - x_t^2\|_2 \geq \sqrt{2}$ for all $t \in [T]$. The demonstrations are plotted in Fig. 12.

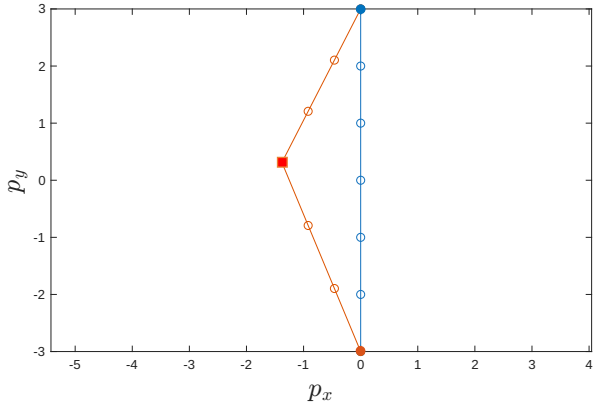


Fig. 12: A demonstration of two interacting dynamic agents with spherical collision-avoidance constraints of different radii: 1 for Agent 1 (blue) and $\sqrt{2}$ for Agent 2 (red). Constraint learning via the centralized, single-agent approach characterized by (75) produced a stationarity error of 2.5.

7) Nonlinear Constraint Recovery: We also evaluate our method on simulated interactions between agents with single-integrator dynamics subject to *a priori* unknown constraints that are nonlinear in the state and control variables (but affine in the unknown constraint parameter θ). We also report the Gurobi solve times, for learning spherical collision-avoidance constraints, as a function of the number of interacting agents. Below, we provide the ground truth parameters and other details of the aforementioned experiments that were omitted in the main text.

a) Nonlinear Constraint Recovery under Cost Certainty: We generate, in simulation, an interaction demonstration of two agents whose motion satisfies single integrator dynamics discretized at intervals of $\Delta t = 0.5$, as well as the following parameterized constraints:

$$\bigwedge_{t=1}^T \bigwedge_{j \in [N] \setminus \{i\}} \left\{ 2(p_{x,t}^j - p_{x,t}^i)^4 + 2(p_{y,t}^j - p_{y,t}^i)^4 - 5(p_{x,t}^j - p_{x,t}^i)^3 - 5(p_{y,t}^j - p_{y,t}^i)^3 \right. \quad (76)$$

$$\left. + 5(p_{x,t}^j - p_{x,t}^i - 1)^3 + 5(p_{y,t}^j - p_{y,t}^i + 1)^3 - \theta_8^i \leq 0 \right\}.$$

We set the following ground truth parameter values, which are *a priori* unknown to the constraint learner, as follows:

$$\theta_8^i = 2, \quad \forall i \in \{1, 2\}. \quad (77)$$

To generate the interaction demonstration, we set the time horizon to be $T = 50$ and define the cost function J^i as follows:

$$J^i = \sum_{t=1}^T \sum_{j=1}^2 \left(\|p_{t+1}^j - p_t^j\|_2^2 + \|u_t^j\|_2^2 \right). \quad (78)$$

The start and goal positions of each agent $i \in [2]$ are constrained via known equality constraints of the form (71) to be at \bar{p}_o^i and \bar{p}_d^i , respectively, as given below:

$$\begin{aligned} \bar{p}_o^1 &= (-2.0, -2.0), & \bar{p}_d^1 &= (-1.0, -0.2), \\ \bar{p}_o^2 &= (2.0, 2.0), & \bar{p}_d^2 &= (3.0, 0.5). \end{aligned}$$

We successfully recovered the *a priori* unknown constraint parameters with a Gurobi solve time of 0.02 seconds. The generated demonstration interactions are provided in Fig. 13a and 13b. The learned constraints were then used to generate safe motion plans in simulation, in conjunction with the agent costs, dynamics, time discretization, and time horizon given above, as well as equality constraints of the form (71) to enforce the following start positions \bar{p}_o^i and goal positions \bar{p}_d^i for each agent i :

$$\begin{aligned} \bar{p}_o^1 &= (3.0, -2.0), & \bar{p}_d^1 &= (-3.0, 2.0), \\ \bar{p}_o^2 &= (-3.0, 2.0), & \bar{p}_d^2 &= (3.0, -2.0). \end{aligned}$$

The generated safe motion plans are plotted in Figs. 13c and 13d.

b) Nonlinear Constraint Recovery under Cost Uncertainty: We repeat the above nonlinear constraint learning and motion planning simulations, with all parameters (including start and goal positions) held fixed, for the setting where the cost objectives of the agents, denoted \bar{J}^1 and \bar{J}^2 below, are also characterized by parameters $\bar{\theta}_1^1$ and $\bar{\theta}_2^2$ whose ground truth values are *a priori* unknown by the constraint learners. Specifically, we assume here that the agents' cost functions are given by:

$$\begin{aligned} \bar{J}^i(\bar{\theta}^i) &= \sum_{t=1}^T \left(\|p_{t+1}^1 - p_t^1\|_2^2 + \bar{\theta}^i \|p_{t+1}^2 - p_t^2\|_2^2 \right) \\ &\quad + \sum_{t=1}^T \sum_{j=1}^2 \|u_t^j\|_2^2, \quad \forall i \in \{1, 2\}, \end{aligned} \quad (79)$$

with ground truth parameter values $\bar{\theta}^i = 0.73$ for each $i \in \{1, 2\}$. We successfully recovered the *a priori* unknown constraint parameters with a Gurobi solve time of 0.03 seconds. The generated demonstration interactions are provided in Fig. 13a and 13b. The learned constraints were then used to generate safe motion plans in simulation, in conjunction

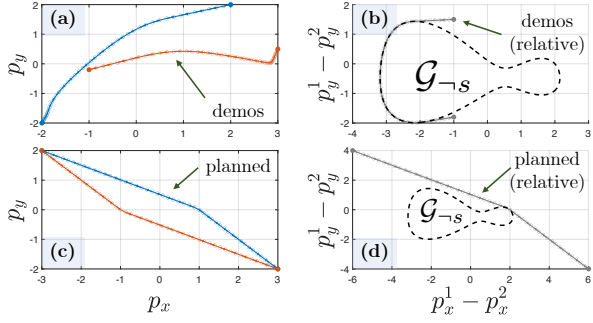


Fig. 13: Constraint learning and safe planning for Agents 1 (blue) and 2 (red) with single integrator dynamics satisfying nonlinear constraints characterized by *a priori* unknown parameters. (a) A demonstration of Agents 1 and 2, in relative coordinates, operating in a shared environment while satisfying their nonlinear constraints. (b) Our method exactly recovers the *a priori* unknown constraint parameters of each agent. We have overlaid the true unsafe set $\mathcal{A}(\theta^*)$ which coincides with the guaranteed learned unsafe set $\mathcal{G}_{\gamma_s}(\mathcal{D})$. (c) Using our learned constraints, we generate safe motion plans via volume extraction over the trajectory space. (d) We plot our generated safe motion plans overlaid with $\mathcal{A}(\theta^*)$ and $\mathcal{G}_{\gamma_s}(\mathcal{D})$.

with the agent costs, dynamics, time discretization, and time horizon given above, as well as equality constraints of the form (71) to enforce the following start positions \bar{p}_o^i and goal positions \bar{p}_d^i for each agent i :

$$\begin{aligned} \bar{p}_o^1 &= (3.0, -2.0), & \bar{p}_d^1 &= (-3.0, 2.0), \\ \bar{p}_o^2 &= (-3.0, 2.0), & \bar{p}_d^2 &= (3.0, -2.0). \end{aligned}$$

The generated safe motion plans are plotted in Figs. 13c and 13d.

8) *Hardware Experiments*: As described in Sec. V-G, we evaluate our method on hardware experiments between ground robots with unicycle dynamics and either spherical or polytopic collision-avoidance constraints, as described by (61) and (63). Below, we provide the ground truth parameters and other details of the aforementioned experiments that were omitted in the main text.

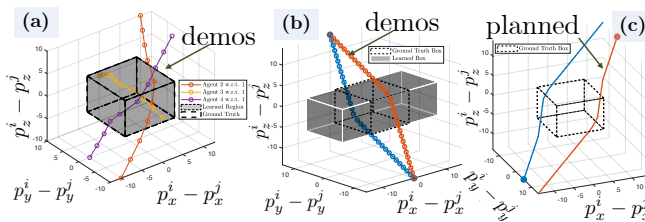


Fig. 14: Constraint learning for quadcopter agents with box constraints, from a demonstration with (a) 4 agents, from which the constraint was recovered, or (b) 2 agents, which fails to activate some constraints that were thus not learned. (c) Regardless, our method generated safe plans via volume extraction over trajectory space.

a) *Spherical Collision-Avoidance Constraints*: We generate three interaction demonstrations of two ground robots, which we then use to learn their spherical collision-avoidance constraint sets (Fig. 3a). The three interaction demonstrations share all of the following parameter settings presented below, including the two robots' initial and final goal positions. Specifically, we discretize the continuous-time unicycle dynamics (55) at intervals of $\Delta t = 1$, and set the time horizon to be $T = 33$. We define the cost of each agent to encode the smoothness objective formulated in Sec. V-A, i.e.,

$$J^i = \sum_{t=1}^{T-1} \|p_{t+1}^i - p_t^i\|_2^2, \quad \forall i \in \{1, 2\}.$$

Spherical collision-avoidance constraints of the form (61), with the following *a priori* unknown ground truth parameters, are enforced on the agents' trajectories:

$$\theta_1^1 = 0.55, \quad \theta_2^2 = 0.55.$$

The start and goal positions of each agent $i \in [2]$ are constrained via known equality constraints of the form (71) to be at \bar{p}_o^i and \bar{p}_d^i , respectively, as given below:

$$\begin{aligned} \bar{p}_o^1 &= (0.8, -0.8), & \bar{p}_d^1 &= (-0.8, 0.8), \\ \bar{p}_o^2 &= (-0.8, 0.8), & \bar{p}_d^2 &= (0.8, -0.8). \end{aligned}$$

We successfully recovered the *a priori* unknown constraint parameters with a Gurobi solve time of 0.03 seconds. The learned constraints were then used to generate two safe motion plans on our hardware setup, in conjunction with the agent costs, dynamics, time discretization, and time horizon given above, but different start positions \bar{p}_o^i and goal positions \bar{p}_d^i for each agent i , as enforced by equality constraints of the form (71). In particular, for the first motion plan, we set:

$$\begin{aligned} \bar{p}_o^1 &= (-0.7, -0.7), & \bar{p}_d^1 &= (0.7, 0.7), \\ \bar{p}_o^2 &= (-0.7, 0.7), & \bar{p}_d^2 &= (0.7, -0.7). \end{aligned}$$

For the second motion plan, we set:

$$\begin{aligned} \bar{p}_o^1 &= (0.7, -0.7), & \bar{p}_d^1 &= (-0.7, 0.7), \\ \bar{p}_o^2 &= (-0.7, 0.7), & \bar{p}_d^2 &= (0.7, -0.7). \end{aligned}$$

Both motion plans are plotted in Fig. 3b.

b) *Box-Shaped Collision-Avoidance Constraints*: We generate two interaction demonstrations of two ground robots, which we then use to learn their polytopic collision-avoidance constraint sets (Fig. 3c). The two interaction demonstrations share all of the following parameter settings presented below, including the two robots' initial and final goal positions. Specifically, we discretize the continuous-time quadcopter dynamics at intervals of $\Delta t = 1$, and set the time horizon to be $T = 33$. We define the cost of each agent to encode the smoothness objective formulated in Sec. V-A, i.e.,

$$J^i = \sum_{t=1}^{T-1} \|p_{t+1}^i - p_t^i\|_2^2, \quad \forall i \in \{1, 2\}.$$

Polytopic collision-avoidance constraints of the form (63) with the *a priori* unknown ground truth parameters $\{a_\beta(\theta)\}$ \in

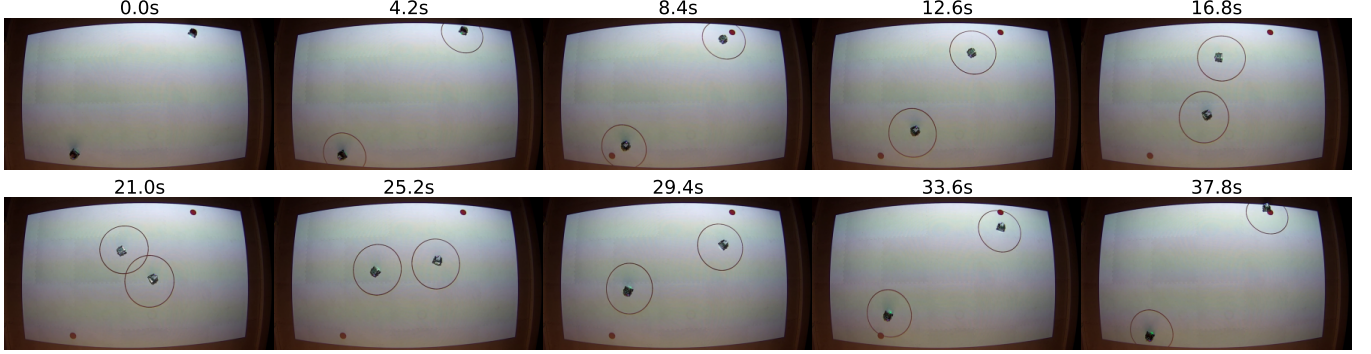


Fig. 15: A time-lapse montage of an interaction demonstration between two ground robots in our hardware setup. Here, both robots follow unicycle dynamics and obey spherical collision-avoidance constraints.

$\mathbb{R}^2, b_\beta(\theta) \in \mathbb{R} : \beta \in [4]\}$ defined below, are enforced on each agent's trajectory. For each $\beta \in [6]$, we set $a_\beta(\theta) \in \mathbb{R}^2$ to be the transpose of the β -th row of the matrix $A(\theta)$ defined below, and we set $b_\beta(\theta) \in \mathbb{R}$ to be the β -th entry of the vector $b(\theta)$ defined below:

$$A(\theta) = \begin{bmatrix} 1.0 & 0.0 \\ -1.0 & 0.0 \\ 0.0 & 1.0 \\ 0.0 & -1.0 \end{bmatrix}, \quad b(\theta) = \begin{bmatrix} -0.4 \\ -0.4 \\ -0.2 \\ -0.2 \end{bmatrix}.$$

The start and goal positions of each agent $i \in [2]$ are constrained via known equality constraints of the form (71) to be at \bar{p}_o^i and \bar{p}_d^i , respectively, as given below:

$$\begin{aligned} \bar{p}_o^1 &= (0.8, -0.8), & \bar{p}_d^1 &= (-0.8, 0.8), \\ \bar{p}_o^2 &= (-0.8, 0.8), & \bar{p}_d^2 &= (0.8, -0.8). \end{aligned}$$

We successfully recovered the *a priori* unknown constraint parameters with a Gurobi solve time of 0.23 seconds. The learned constraints were then used to generate two safe motion plans on our hardware setup, in conjunction with the agent costs, dynamics, time discretization, and time horizon given above, but different start positions \bar{p}_o^i and goal positions \bar{p}_d^i for each agent i , as enforced by equality constraints of the form (71). In particular, for the first motion plan, we set:

$$\begin{aligned} \bar{p}_o^1 &= (-0.7, -0.7), & \bar{p}_d^1 &= (0.7, 0.7), \\ \bar{p}_o^2 &= (-0.7, 0.7), & \bar{p}_d^2 &= (0.7, -0.7). \end{aligned}$$

For the second motion plan, we set:

$$\begin{aligned} \bar{p}_o^1 &= (0.7, -0.7), & \bar{p}_d^1 &= (-0.7, 0.7), \\ \bar{p}_o^2 &= (-0.7, 0.7), & \bar{p}_d^2 &= (0.7, -0.7). \end{aligned}$$

Both motion plans are plotted in Fig. 3d.

9) *Comparison Against the Cost Inference Baseline:* As described in Sec. V-H, we compared our constraint-learning based approach for safe motion planning against the cost inference-based baseline approach in [4]. Concretely, we first generated an interaction demonstration of two agents with double integrator dynamics discretized at intervals of $\Delta t = 1$, who interact over a time horizon of $T = 10$. When generating the interaction demonstration, we define the cost

of each agent to encode the smoothness objective formulated in Sec. V-A, i.e.,

$$J^i = \sum_{t=1}^{T-1} \|p_{t+1}^i - p_t^i\|_2^2, \quad \forall i \in \{1, 2\}.$$

Spherical collision-avoidance constraints of the form (61) with *a priori* unknown ground truth parameters θ_1^1 and θ_1^2 as given below, are enforced on each agent's demonstration trajectory:

$$\theta_1^i = 49, \quad \forall i \in \{1, 2\}. \quad (80)$$

The start and goal positions of each agent $i \in [2]$ are constrained via known equality constraints of the form (71) to be at \bar{p}_o^i and \bar{p}_d^i , respectively, as given below:

$$\begin{aligned} \bar{p}_o^1 &= (0.0, 0.0), & \bar{p}_d^1 &= (10.0, 10.0), \\ \bar{p}_o^2 &= (10.0, 10.0), & \bar{p}_d^2 &= (0.0, 0.0). \end{aligned}$$

Our constraint learning method successfully recovered the *a priori* unknown constraint parameters with a Gurobi solve time of 0.04 seconds. Meanwhile, the baseline method extracts each agents' collision-avoidance intent by attempting to learn the parameter $\tilde{\theta}$ in the following cost function (first presented in Sec. V-H), which encodes collision-avoidance as a log-barrier function. Note that the baseline method does not assume that hard collision-avoidance constraints are enforced on either agent's trajectory:

$$\begin{aligned} \tilde{J}^i(\tilde{\theta}) &:= J^i - \tilde{\theta} \cdot \sum_{t=1}^T \log(\|p_t^i - p_t^{2-i}\|_2^2) \\ &= \sum_{t=1}^{T-1} \|p_{t+1}^i - p_t^i\|_2^2 - \tilde{\theta} \cdot \sum_{t=1}^T \log(\|p_t^i - p_t^{2-i}\|_2^2). \end{aligned} \quad (81)$$

Using the baseline method, we recover the parameter $\tilde{\theta} = 2.51$.

We compare the safety guarantees of motion plans generated using our learned constraints against motion plans generated using the baseline method. Specifically, we first generate motion plans via our method, using (1) the smoothness cost (73), (2) the spherical collision-avoidance constraints (61) with the recovered constraint parameters $\theta_1^1 = \theta_1^2 = 49$, i.e.,

(80), and (3) equality constraints of the form (71) to encode the start positions \bar{p}_o^i and goal positions \bar{p}_d^i of each agent $i \in \{1, 2\}$:⁹

$$\begin{aligned}\bar{p}_o^1 &= (0.0, 5.0), & \bar{p}_d^1 &= (10.0, 5.0), \\ \bar{p}_o^2 &= (10.0, 5.0), & \bar{p}_d^2 &= (0.0, 5.0).\end{aligned}$$

Next, we generate motion plans via the baseline approach, using the smoothness plus log barrier cost (81) with inferred parameter $\tilde{\theta} = 2.51$, *without any hard collision-avoidance constraints*. As noted in Sec. V-H and Fig. 7, the motion plan generated using our method (and our learned constraints) satisfies the ground truth spherical collision-avoidance constraint, while the motion plan generated using the baseline approach violates the ground truth spherical collision-avoidance constraint.

⁹Note that Fig. 7a shows the forward motion plans generated in *relative* coordinates, whereas the start and goal positions reported here are in *absolute* coordinates.